Heteroatom modified polymer immobilized ionic liquid stabilized ruthenium nanoparticles: efficient catalysts for the hydrolytic evolution of hydrogen from sodium borohydride

Paterson, R. ORCID: https://orcid.org/0000-0002-9237-6130, Alharbi, A. A. ORCID: https://orcid.org/0000-0001-7189-2008, Wills, C. ORCID: https://orcid.org/0000-0002-6571-2389, Dixon, C., Šiller, L., Chamberlain, T. W. ORCID: https://orcid.org/0000-0001-8100-6452, Griffiths, A., Collins, S. M. ORCID: https://orcid.org/0000-0002-5151-6360, Wu, K., Simmons, M. D. ORCID: https://orcid.org/0000-0001-7598-7266, Bourne, R. A., Lovelock, K. R. J. ORCID: https://orcid.org/0000-0003-1431-269X, Seymour, J., Knight, J. G. ORCID: https://orcid.org/0000-0002-1120-8259 and Doherty, S. ORCID: https://orcid.org/0000-0003-1103-8090 (2022) Heteroatom modified polymer immobilized ionic liquid stabilized ruthenium nanoparticles: efficient catalysts for the hydrolytic evolution of hydrogen from sodium borohydride. Molecular Catalysis, 528. 112476. ISSN 2468-8231 doi: 10.1016/j.mcat.2022.112476 Available at https://centaur.reading.ac.uk/106704/

Published version at: http://dx.doi.org/10.1016/j.mcat.2022.112476
To link to this article DOI: http://dx.doi.org/10.1016/j.mcat.2022.112476

Publisher: Elsevier

Molecular Catalysis 528 (2022) 112476

Contents lists available at ScienceDirect

Molecular Catalysis

journal homepage: www.journals.elsevier.com/molecular-catalysis

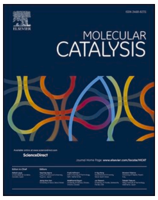

Heteroatom modified polymer immobilized ionic liquid stabilized ruthenium nanoparticles: Efficient catalysts for the hydrolytic evolution of hydrogen from sodium borohydride**

Reece Paterson[a], Adhwa A. Alharbi[a], Corinne Wills[a], Casey Dixon[a], Lidja Šiller[b], Thomas W. Chamberlain[c,*], Anthony Griffiths[c], Sean M. Collins[c], Kejun Wu[c], Matthew D. Simmons[c], Richard A. Bourne[c], Kevin R.J. Lovelock[d], Jake Seymour[d], Julian G. Knight[a], Simon Doherty[a,*]

[a] Newcastle University Centre for Catalysis (NUCAT), School of Chemistry, Bedson Building, Newcastle University, Newcastle upon Tyne NE1 7RU, UK
[b] School of Engineering, Bedson Building, Newcastle University, Newcastle upon Tyne NE1 7RU, UK
[c] Institute of Process Research & Development School of Chemistry and School of Chemical and Process Engineering, University of Leeds, Woodhouse Lane LS2 9JT, UK
[d] School of Chemistry, Food and Pharmacy, University of Reading, Reading RG6 6AT, UK

ARTICLE INFO

Keywords:
Sodium borohydride
Catalytic hydrogen generation
Ruthenium nanoparticles
Kinetics and deuterium labelling
Recycle and catalyst poisoning

ABSTRACT

Ruthenium nanoparticles stabilised by polymer immobilized ionic liquids catalyse the hydrolytic release of hydrogen from sodium borohydride. The composition of the polymer influences performance and ruthenium nanoparticles stabilised by an amine-decorated imidazolium-based polymer immobilised ionic liquid (RuNP@NH_2-PIILS) was the most efficient with a maximum initial turnover frequency (TOF) of 177 $mole_{H2}.mol_{Ru}^{-1}.min^{-1}$, obtained at 30°C with a catalyst loading of 0.08 mol%; markedly higher than that of 69 $mol_{H2}.mol_{Ru}^{-1}.min^{-1}$ obtained with 5 wt% Ru/C and one of the highest to be reported for a RuNP catalyst. The apparent activation energy (Ea) of 38.9 kJ mol^{-1} for the hydrolysis of $NaBH_4$ catalysed by RuNP@NH_2-PIILS is lower than that for the other polymer immobilized ionic liquid stabilised RuNPs, which is consistent with its efficacy. Comparison of the initial rates of hydrolysis in H_2O and D_2O catalysed by RuNP@NH_2-PIILS gave a primary kinetic isotope effect (k_H/k_D) of 2.3 which supports a mechanism involving rate limiting oxidative addition of one of the O-H bonds in a strongly hydrogen-bonded surface-coordinated $[BH_3H^-]$—-H_2O ensemble. The involvement of a surface-coordinated borohydride is further supported by an inverse kinetic isotope effect of 0.65 obtained from a comparison of the initial rates for the hydrolysis of $NaBH_4$ and $NaBD_4$ under the conditions of catalysis i.e., at a high hydride/catalyst mole ratio. Interestingly though, when the comparison of the initial rates of hydrolysis of $NaBH_4$ and $NaBD_4$ was conducted in dilute solution with a hydride/catalyst mole ratio of 1 a kinetic isotope effect (k_H/k_D) of 2.72 was obtained; this would be more consistent with concerted activation of both an O-H and B-H bond in the rate limiting step, possibly via a concerted oxidative addition-hydride transfer in the surface-coordinated hydrogen-bonded ensemble. Catalyst stability and reuse studies showed that RuNP@NH_2-PIILS retained 71% of its activity over five runs; the gradual drop in the initial TOF with run number appears to be due to passivation of the catalyst by the sodium borate by-product as well as an increase in viscosity of the reaction mixture rather than leaching of the catalyst.

1. Introduction

There is an increasing urgency to identify alternative energy sources to fossil fuels in order to meet the need to supply sustainable, clean energy as well as reduce greenhouse emissions to mitigate rising global temperatures, extreme and fluctuating weather patterns, and the negative impact on the earth's ecosystem [1–4]. To this end, hydrogen is an attractive energy carrier as a source of clean efficient power in

---

** This article is dedicated to the memory of Professor Stephen A. Westcott

* Corresponding authors.
E-mail addresses: t.w.chamberlain@leeds.ac.uk (T.W. Chamberlain), simon.doherty@ncl.ac.uk (S. Doherty).

https://doi.org/10.1016/j.mcat.2022.112476
Received 13 May 2022; Received in revised form 23 June 2022; Accepted 24 June 2022

stationary, portable and transport applications [5] as it has a high energy density (142 MJ·kg^{-1} *vs* 54 MJ·kg^{-1} for natural gas) as well as the potential to be generated in high purity from water splitting where the only by-product is oxygen [6–12]. However, hydrogen is a flammable gas which forms potentially explosive environments and, as such, there are significant safety concerns over its storage and transportation; moreover, compression and liquefaction of hydrogen are energy intensive processes. The use of hydrogen storage materials is one of the most promising solutions as they are stable and safe to handle and would allow for the generation of hydrogen on site [6,13-25]. To this end, sodium borohydride has appropriate credentials for use as a storage material as it has a high stability and a high hydrogen content (10.8 wt %) and is nontoxic, inexpensive and water soluble (Eq. 1) [6,13b,c,j,k, 25-32].

$$NaBH_4 + 4H_2O \rightarrow NaB(OH)_4 + 4H_2 \quad (1)$$

As the thermal decomposition of $NaBH_4$ requires temperatures in excess of 400°C and its hydrolysis in water is slow, considerable effort has been dedicated to developing cost-effective catalysts that can achieve the rapid and controllable release of hydrogen that will be required for this technology to become commercially viable. While homogeneous catalysts have been shown to facilitate the solvolysis of hydrogen-rich boron compounds [33–38], noble metal nanoparticles (NPs) have recently attracted considerable attention as the hydrogen generation rate can be controlled through their size, morphology and environment and the catalyst can be recovered and reused in much the same manner as a conventional heterogeneous catalyst [39–43]. While the high activity obtained with small nanoparticles is due to their high surface area to volume ratio and the large number of active sites, they are unstable with respect to aggregation to less reactive species which limits their practical applications [44–45], for example, integration into hydrogen-based fuel cells for use in vehicles and portable electronic devices [46–48]. One potential solution to overcome aggregation under conditions of catalysis has been to stabilise the nanoparticles by encapsulation into a support such as porous carbon structures [49–60], zeolites [61–65], mesoporous silicas [66–68], porous organic polymers [69–70], metal organic frameworks [71–77] and, most recently, dendrimers [78–80]. Additional benefits of this strategy include control of the growth and morphology due to the confinement [81–87], modification of their properties through surface-support interactions [88–93] and incorporation of functionality to affect synergy, for instance, bimetallic nanoparticles [94–97]. At present, the most efficient supported NP catalyst for the hydrolysis of sodium borohydride is based on RuNPs confined in zeolite-Y; this system gave a turnover frequency of 550 $mol_{H2}.mol_{Ru}^{-1}.min^{-1}$ [64].

Ionic liquids have also been used for the stabilization of nanoparticles [98–101]; however, the weak electrostatic interactions involved do not always provide sufficient stabilisation to prevent aggregation under the conditions of catalysis [102–103]. One possible approach to improve nanoparticle stability has been to introduce a heteroatom donor such as a phosphine, amine, nitrile, ether, or thiol that can supplement this weak stabilization by forming a covalent interaction to the nanoparticle surface [104]. This approach has proven successful with significant improvements in catalyst stability and performance; for example, palladium nanoparticles stabilised by a phosphine-functionalised imidazolium-based ionic liquid are markedly more efficient hydrogenation catalysts than their unmodified counterparts [105–109] while RuNPs stabilised by a phosphine-functionalised ionic liquid exhibited a solvent dependent chemoselectivity for the hydrogenation of aromatic ketones as reactions performed in ionic liquid were highly selective for reduction of the carbonyl group whereas the use of water as the solvent resulted in hydrogenation of both the carbonyl and the arene. Moreover, the phosphine was shown to exert a marked influence on catalyst efficiency as the corresponding phosphine-free RuNP catalyst was markedly less selective in both solvents [110–111]. However, even though this strategy has been shown to improve catalyst performance, functional ionic liquids are prohibitively expensive as a bulk solvent, leaching contaminates the product and recovery, and purification of the ionic liquid can be difficult, which has limited their implementation.

These issues have been addressed by grafting ionic liquids onto supports such as mesoporous silica, polymers, and MOFs on the basis that the resulting material would stabilise the nanoparticles in much the same manner as an ionic liquid, while the covalent attachment would prevent leaching of the ionic liquid, facilitate separation and recovery of the catalyst, and reduce the amount of ionic liquid, as the catalyst would be confined within the support [112–117]. Polymers are particularly attractive supports as their modular construction would enable the hydrophilicity, ionic microenvironment, charge density and redox properties to be modified in a rational manner, additional functionality to be introduced and the composition and stoichiometry of the metal precursors to be defined to facilitate access to synergistic bi- and trimetallic nanoparticles. We have recently been exploring this approach and developed heteroatom donor-decorated polymer-immobilised ionic liquids, reasoning that the heteroatom donor could influence the size, size distribution and morphology of the nanoparticles as well as modify their surface electronic structure and, thereby, modulate their efficacy as catalysts. In this regard, there have been an increasing number of reports of the beneficial effect of ligands on the performance of heterogeneous nano-catalysts, which have been attributed to steric, electronic and solubility factors [118]. Our early studies showed that palladium nanoparticles immobilized on a polyethylene glycol-modified phosphine-modified PIIL is a remarkably efficient catalyst for aqueous phase Suzuki-Miyaura cross-couplings [119], the chemoselective hydrogenation of α,β-unsaturated ketones, nitriles and esters, [120] and the hydrogenation of nitroarenes [121]. Moreover, gold nanoparticles stabilized by a phosphine oxide-modified polymer immobilised ionic liquid catalyses the highly selective reduction of nitroarenes to afford *N*-arylhydroxylamines and azoxyarenes [122] and the corresponding ruthenium nanoparticles catalyse the aqueous phase hydrogenation of aryl and heteroaryl ketones and levulinic acid with remarkable efficacy and selectivity [123].

While support-grafted ionic liquids have been used to stabilise catalysts for a wide range of transformations, there appear to be only two reports of their use to support nanoparticle catalysts for the hydrolytic evolution of hydrogen from hydrogen-rich boron derivatives, which is somewhat surprising as polymer immobilised ionic liquids are functional and tuneable supports for molecular and nanoparticle catalysts. An imidazolium-based organic polymer has recently been used to prepare highly dispersed ultrafine AuPd alloy NPs for the hydrolytic release of hydrogen from ammonia borane which outperformed both its monometallic counterparts [124] and we have recently reported that phosphine decorated polymer immobilized ionic liquid stabilized PtNPs are highly efficient catalysts for the hydrolytic generation of hydrogen from $NaBH_4$ [125]. This study has now been extended to investigate the efficacy of phosphine oxide and amine-decorated polymer immobilised ionic liquid stabilised RuNPs as catalysts for the hydrolysis of $NaBH_4$ on the basis that the heteroatom donor could disrupt the key hydrogen-bonded surface-coordinated ensemble between the acidic hydrogen of water and the hydridic hydrogen of borohydride and thereby influence catalyst performance. Herein, we report the results of a comparative study to explore the influence of polymer composition on catalyst performance and reveal that that RuNPs stabilised by an amino-modified polyionic liquid outperform their phosphine oxide-decorated and unmodified counterparts. Kinetic studies in combination with deuterium isotope effects have been used to probe the mechanism and a tandem hydrogenation of 1,1-diphenylethene with hydrogen generated from the catalytic hydrolysis of $NaBH_4$ in D_2O gave a mixture of isotopologues resulting from reversible β-hydride elimination/re-insertion at a surface Ru-D competing with reductive elimination.

2. Experimental

2.1. Materials

All reagents were purchased from commercial suppliers and used without further purification, $RuCl_3.3H_2O$ 99.9% (PGM basis) was purchased form Alfa Aesar (47182) and polymers **1a-f** were prepared as previously described and their purity confirmed by ^1H and $^{13}C\{^1H\}$ NMR spectroscopy and elemental analysis. Ethanol was distilled over iodine activated magnesium with a magnesium loading of 5.0 g L^{-1} and diethyl ether from Na/K alloy under an atmosphere of nitrogen.

2.2. Preparation of catalysts 2a-f

2.2.1. Synthesis of RuNP@PIILS (2a)

To a round bottom flask charged with **1a** (4.0 g, 6.5 mmol) and ethanol (100 mL) was added a solution of $RuCl_3{\cdot}3H_2O$ (1.3 g, 6.5 mmol) in ethanol (20 mL). The resulting mixture was stirred vigorously for 5 h at room temperature after which time a solution of $NaBH_4$ (2.0 g, 52.0 mmol) in water (10 mL) was added dropwise and the suspension stirred for an additional 18 h before concentrating to dryness under vacuo. The crude black solid was triturated with cold acetone (2 × 100 mL) then washed with water (100 mL) followed by ethanol (2 × 40 mL) to afford a black solid that was recovered from the washings via centrifugation followed by filtration through a frit. The final product was rinsed with ether until a fine black powder was obtained which was dried under vacuum to afford **2a** in 87% yield (4.06 g). ICP-OES data: 5.85 wt% ruthenium and a ruthenium loading of 0.58 mmol•g^{-1}.

2.2.2. Synthesis of RuNP@PEGPIILS (2b)

Catalyst **2b** was prepared from **1b** (1.0 g, 0.83 mmol), $RuCl_3{\cdot}3H_2O$ (0.17 g, 0.83 mmol) and $NaBH_4$ (0.25 g, 6.64 mmol) in ethanol (25 mL) as described above to afford a fine black powder in 50% yield (0.54 g). ICP-OES data: 7.02 wt% ruthenium and a ruthenium loading of 0.70 mmol•g^{-1}.

2.2.3. Synthesis of RuNP@O=PPh_2-PIILS (2c)

Catalyst **2c** was prepared from **1c** (5.0 g, 6.25 mmol), $RuCl_3{\cdot}3H_2O$ (1.30 g, 6.25 mmol) and $NaBH_4$ (1.89 g, 50 mmol) in ethanol (100 mL) as described above to afford a fine black powder in 53% yield (2.82 g). ICP-OES data: 7.24 wt% ruthenium and a ruthenium loading of 0.72 mmol•g^{-1}.

2.2.4. Synthesis of RuNP@O=PPh_2-PEGPIILS (2d)

Catalyst **2d** was prepared from **1d** (4.0 g, 2.68 mmol), $RuCl_3{\cdot}3H_2O$ (0.46 g, 2.68 mmol) and $NaBH_4$ (0.81 g, 21.4 mmol) in ethanol (100 mL) as described above to afford a fine black powder in 78% yield (3.32 g). ICP-OES data: 1.83 wt% ruthenium and a ruthenium loading of 0.18 mmol•g^{-1}.

2.2.5. Synthesis of RuNP@NH_2-PIILS (2e)

Catalyst **2e** was prepared from **1e** (5.0 g, 7.75 mmol), $RuCl_3{\cdot}3H_2O$ (1.60 g, 7.75 mmol) and $NaBH_4$ (2.34 g, 62 mmol) in ethanol (100 mL) as described above to afford a fine black powder in 67% yield (3.88 g). ICP-OES data: 3.43 wt% ruthenium and a ruthenium loading of 0.34 mmol•g^{-1}.

2.2.6. Synthesis of RuNP@NH_2-PEGPIILS (2f)

Catalyst **2f** was prepared from **1c** (4.0 g, 5.11 mmol), $RuCl_3{\cdot}3H_2O$ (1.06 g, 5.11 mmol) and $NaBH_4$ (1.54 g, 40.9 mmol) in ethanol (100 mL) as described above to afford a fine black powder in 79% yield (3.45 g). ICP-OES data: ICP-OES data: 6.97 wt% ruthenium and a ruthenium loading of 0.69 mmol g^{-1}.

2.3. Kinetic studies

2.3.1. Ruthenium nanoparticle-catalyzed hydrolysis of sodium borohydride

Comparative catalytic hydrolysis reactions were conducted in water at the appropriate temperature in a thermostated 50 mL round bottom flask. In a typical experiment, a flask charged with a stir bar, catalyst **2a-f** (0.2 mol%) and $NaBH_4$ (0.021 g, 0.57 mmol) and fitted with a gas outlet and connected to the top of an inverted water-filled burette designed to monitor the progress of the reaction by measuring the volume of water displaced with time. The flask was stabilised at 303 K and the reaction was initiated by adding water (2 mL) and the system was immediately sealed by replacing the gas outlet; the tap to the water filled burette was then opened, the time zero volume recorded, and the water displacement monitored. The optimum activity for each catalyst was determined by varying the catalyst loadings between 0.08 and 0.32 mol % at 303 K and measuring the hydrogen produced as a function of time. Kinetic studies were also conducted according to the protocol described above using the following catalyst loadings: 0.26 mol% **2a**, 0.32 mol% **2b,** 0.45 mol% **2c**, 0.11 mol% **2d**, 0.16 mol% **2e** and 0.32 mol% **2f** for a range of temperatures (294 K, 298 K, 303 K, 308 K and 313 K) and the corresponding activation energies (E_a) were determined from an Arrhenius plot of the initial rate against 1/T.

2.3.2. Reaction order for the RuNP-catalyzed hydrolysis of sodium borohydride

The reaction order in catalyst was determined by performing the hydrolysis reactions at 298 K with $NaBH_4$ (0.28 M, 0.021 g) in water (2 mL) and varying the catalyst concentration from 0.14 mol% to 0.69 mol % for **2a,** 0.16 mol% to 0.63 mol% for **2b**, 0.23 mol% to 1.1 mol% for **2c,** 0.058 mol% to 0.28 mol% for **2d**, 0.12 mol% to 0.27 mol% for **2e** and 0.25 mol% to 0.64 mol% for **2f**. The reaction order in sodium borohydride concentration was investigated by performing reactions at 298 K in water (200 mL) using 0.026 mmol of catalysts **2a** (0.0448 g), **2e** (0.0764 g) and **2f** (0.0376 g) and varying the amount of sodium borohydride between 6.6 μmole and 185 μmole (i.e. $[NaBH_4]_0 = 0.035$, 0.07, 0.13, 0.26, 0.39, 0.53, 0.65, 0.78, 0.9 mM), such that the catalyst:$NaBH_4$ mole ratios ranged from 4:1 and 1:6. The effect of sodium borohydride concentration on the initial rate of hydrolysis at high concentrations of sodium borohydride, *i.e.* under the conditions of catalysis, was also determined using **2e** (0.0026 g, 0.884 μmol) to catalyze the hydrolysis of $NaBH_4$ solutions (2 mL) with varying concentrations of sodium borohydride ranging from 0.55 mmol to 2.2 mmol ($[NaBH_4]_0 = 0.28$, 0.56, 0.83, 1.1 M).

2.3.3. Study of the catalytic efficiency as a function of the concentration of NaOH

The effect of the concentration of NaOH on catalyst efficacy was explored by conducting catalytic hydrolysis reactions at 303 K in 2 mL of alkaline 0.28 M $NaBH_4$ (0.021 g) across a range of sodium hydroxide concentrations (i.e. [NaOH] = 0.035, 0.07, 0.14, 0.28, 5.0, 10, 50, 100 mM) catalyzed by 0.26 mol% **2a** (0.0025 g) and monitoring the gas evolution.

2.4. Catalyst recycle studies

Recycle studies were performed at 303 K as described above using 2 mol% **2a** (0.0193 g, 0.0114 mmol) and **2e** (0.0335 g, 0.0114 mmol) to catalyze the hydrolysis of sodium borohydride (0.021 g, 0.57 mmol) in water (20 mL). The progress of the reaction was monitored as described above and when the hydrolysis was complete an additional portion of fresh sodium borohydride (0.021 g, 0.57 mmol) was added, and the procedure repeated. After the 5th run samples of the catalysts were isolated and analysed by TEM.

2.5. Catalyst recycle studies in the presence of buffer

A borate-buffered solution was prepared by dissolving $Na_2B_4O_7{\cdot}10H_2O$ (9.53 g, 25 mmol) and NaCl (4.39 g, 75 mmol) in distilled water (900 mL) in a volumetric flask. When the borate was completely dissolved the pH of the solution was adjusted to 7.2 by gradual addition of boric acid (20.99 g, 0.34 mol); the solution was then made up to one liter. Recycle studies were conducted by adding $NaBH_4$ (0.021 g, 0.57 mmol) to a flask containing 1 mol% **2e** (0.0165 g, 0.0056 mmol) and 20 mL of the aqueous borate buffer solution. The flask was maintained at 303 K and the progress of the reaction was monitored as described above. When the hydrolysis was complete an additional portion of fresh sodium borohydride (0.021 g, 0.57 mmol) was added, and the procedure repeated for comparison with the recycle study described above in the absence of buffer.

2.6. Hot filtration tests

Hot filtration studies were conducted at 303 K following the protocol described above using either 0.2 mol% **2a** (0.0019 g) or 0.16 mol% **2e** (0.0026 g) to catalyze the hydrolysis of sodium borohydride (0.021 g, 0.57 mmol) in water (2 mL). The progress of the reaction was monitored as a function of time and the mixture filtered through a 0.45 μm syringe filter when the conversion reached *ca*. 50% (10 min for **2a** and 7.75 min for **2e**), after which the burette assembly was reconnected, and the gas evolution monitored for a further 30 min. In a complementary procedure, a hydrolysis reaction that had reached completion was filtered through a 0.45 μm syringe filter and an additional portion of $NaBH_4$ (0.021 g, 0.57 mmol) added to the filtrate and the gas evolution monitored.

2.7. Catalyst poisoning study

A flask was charged with 2 mol% catalyst (**2a** 0.0186 g; **2e**, 0.0335 g), water (20 mL) and sodium metaborate (0.0765 g, 0.57 mmol) and the resulting mixture stirred at 303 K for the predetermined time ($t = 0$ min, 20 min, 40 min, 60 min) to investigate whether the pre-stirring time influences catalyst efficacy. After pre-stirring for the allocated time, the reaction was initiated by addition of the $NaBH_4$ (0.021 g, 0.57 mmol) and the rate of hydrogen evolution quantified by measuring the volume of water displaced with time.

2.8. Tandem hydrogenation of 1,1-diphenylethene

Tandem hydrogenations were performed using two Schlenk flasks connected through tubing. One of the flasks was charged with a stir bar, either $NaBH_4$ (0.042 g, 1.11 mmol) or $NaBD_4$ (0.046 g, 1.11 mol) and 0.26 mol% **2e** (0.0025 g) and the hydrolysis started by addition of either D_2O (2 mL) or H_2O (2 mL). The reaction flask was immediately stoppered, isolated from the second flask by closing the stopcock and stirred for 70 min. The second Schlenk flask was charged with 1,1-diphenylethene (0.180 g, 1.00 mmol), 0.5 mol% Pd/C and either CH_3OH (2 mL) or d_4-methanol (2 mL). After 70 min the second flask was evacuated briefly before opening the connector to the hydrolysis flask. The reaction was allowed to stir at 303 K for 18 h before the solvent was removed and the residue analyzed by $^{13}C\{^1H\}$ NMR spectroscopy and GC-MS to establish the composition and quantify the distribution of isotopologues.

3. Results and discussion

3.1. Catalyst synthesis, characterisation and RuNP-catalyzed hydrolysis of sodium borohydride

The polymers required for this study were prepared *via* radical polymerisation of the corresponding imidazolium-based ionic liquid monomer, either styrene, (4-vinylphenyl)methanamine or diphenyl(4-vinylphenyl)phosphine oxide and the corresponding imidazolium-based ionic liquid cross-linker in the ratio $x = 1.84$, $y = 1.0$ and $z = 0.16$, as previously described [119–123]. Catalysts **2a-f** were prepared by the wet impregnation of the polymer support with ruthenium trichloride to afford precursors with a 1:1 ratio of ruthenium to neutral monomer, followed by *in-situ* reduction of the ruthenium with $NaBH_4$; to afford the product as a fine black powder in high yield; the synthesis and composition of the polymers and the catalysts is shown in Fig. 1. The composition and purity of polymers **1a-f** was determined using a combination of solution and solid state $^{13}C\{H\}$ and $^{31}P\{H\}$ NMR spectroscopy and elemental analysis while the loaded RuNP catalysts were characterised by solid state $^{13}C\{H\}$ and $^{31}P\{H\}$ NMR spectroscopy, infra-red (IR) spectroscopy, high resolution transmission electron microscopy (HRTEM), SEM, X-ray photoelectron spectroscopy (XPS) and inductively coupled plasma-optical emission spectroscopy (ICP-OES) (See Fig. 2 and the supporting information for full details). The ruthenium loadings in **2a-f** were determined to be $0.18-0.75$ $mmolg^{-1}$ using ICP-OES.

The solid state $^{13}C\{^1H\}$ NMR spectra of **1a-f** and **2a-f** each contain resonances from δ 121 to 149 ppm, which correspond to the aromatic carbon atoms of polystyrene and the carbon atoms of the imidazolium ring, as well as signals between δ 10 and 51 ppm which belong to the methylene carbon atoms of the polystyrene backbone and the methyl group attached to the imidazolium ring. Additional signals at δ 71 and 59 ppm for **2b, 2d** and **2f** belong to the carbon atoms of the polyethylene glycol (PEG) chain and the terminal OMe, respectively, and a signal at δ 49 ppm for **2e** and **2f** is associated with the CH_2NH_2. The surface of the RuNP catalysts was characterised by X-ray photoelectron spectroscopy by analysing the Ru 3p region as the C 1s and Ru 3d region overlapped. For catalyst **2a**, stabilised by unmodified imidazolium-based polymer, a Ru $3p_{3/2}$ peak at 463.19 eV was assigned to RuO_2, and satellite features were fitted at 465.97 eV (Table S2 and Fig. 2a). The presence of RuO_2 species is most likely due to surface oxidation of the pre-formed metallic Ru nanoparticles. The corresponding Ru $3p_{3/2}$ peak for catalysts containing the phosphine oxide (**2c** and **2d**) or amine (**2e** and **2f**) was shifted to lower binding energy (462.56 and 461.37 eV for **2c** and **2d**, respectively and 462.83 and 462.89 eV for **2e** and **2f**, respectively) compared to the Ru $3p_{3/2}$ binding energy of 463.19 eV for catalyst **2a** (Table S2 and Fig. 2b-f). A shift to lower binding energy may be indicative of electron transfer from the heteroatom of the phosphine oxide or amine to the RuNPs. Catalyst **2d** containing $O{=}PPh_2$ and PEG heteroatom donors gave the largest shift (-1.72 eV) in binding energy of the Ru $3p_{3/2}$ peak (461.37 eV for **2d**) relative to **2a**. TEM micrographs of **2a-f** revealed that the ruthenium nanoparticles were ultrafine and near monodisperse with average diameters between 1.6 and 2.8 nm; representative micrographs and the corresponding distribution histograms based on the sizing of >100 particles for **2a-f** are shown in Fig. 2. SEM images revealed that the catalyst materials were far more granular than their polymeric counterparts, which appeared largely smooth.

The hydrolysis of sodium borohydride was identified to investigate the efficacy of catalyst **2a-f** on the basis that PEG-modified 'click'-dendrimer stabilised noble and bimetallic metal nanoparticles catalyse this reaction with promising initial TOFs and as such would provide a formative benchmark for comparative evaluation. Preliminary catalyst testing was conducted using recent literature protocols as a lead [75,78]; reactions were initially performed at 303 K using 0.2 mol% of **2a-f** to catalyse the hydrolysis of a 0.28 M solution of sodium borohydride (Fig. 3a, b). The reaction was monitored by quantifying the amount of hydrogen liberated as a function of time using water displacement from an inverted burette assembly and all data were corrected by subtracting the background hydrogen generated over the same time under identical conditions. Hydrogen evolution started immediately with no induction period which is consistent with the metallic state of the ruthenium. Under these conditions, RuNP@NH_2-PIILS (**2e**) gave the highest initial TOF of 135 $mole_{H2}.mol_{Ru}^{-1}.min^{-1}$ and reached 92% conversion after 20 min, whereas its PEGylated counterpart RuNP@NH_2-PEGPIILS (**2f**) was

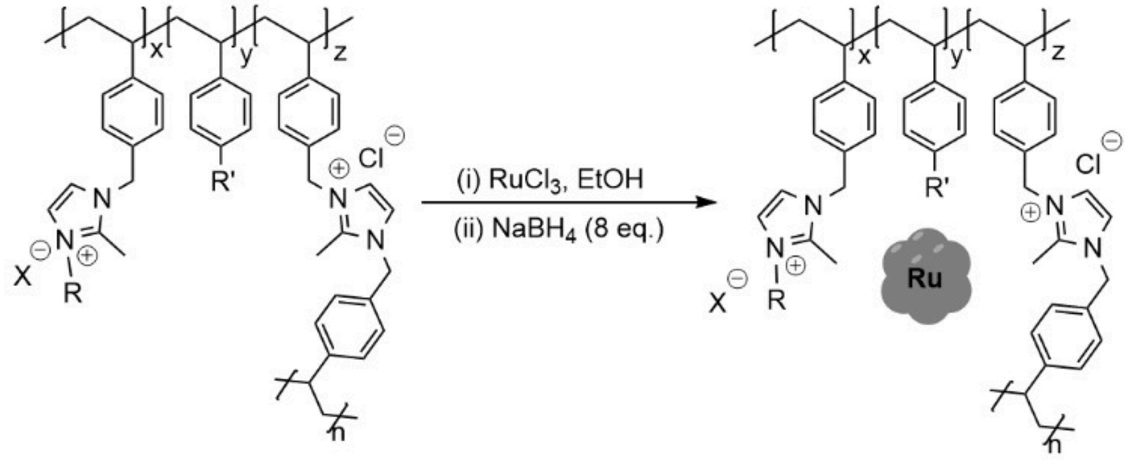

Catalyst	R	R'	X	.
RuNP@PIILS	Me	H	Cl	**2a**
RuNP@PEGPIILS	PEG_{350}	H	Br	**2b**
RuNP@O=PPh_2-PIILS	Me	O=PPh_2	Cl	**2c**
RuNP@O=PPh_2-PEGPIILS	PEG_{350}	O=PPh_2	Br	**2d**
RuNP@NH_2-PIILS	Me	CH_2NH_2	Cl	**2e**
RuNP@NH_2-PEGPIILS	PEG_{350}	CH_2NH_2	Br	**2f**

Fig. 1. Synthesis and composition of PIIL-stabilized ruthenium nanoparticles **2a-f**.

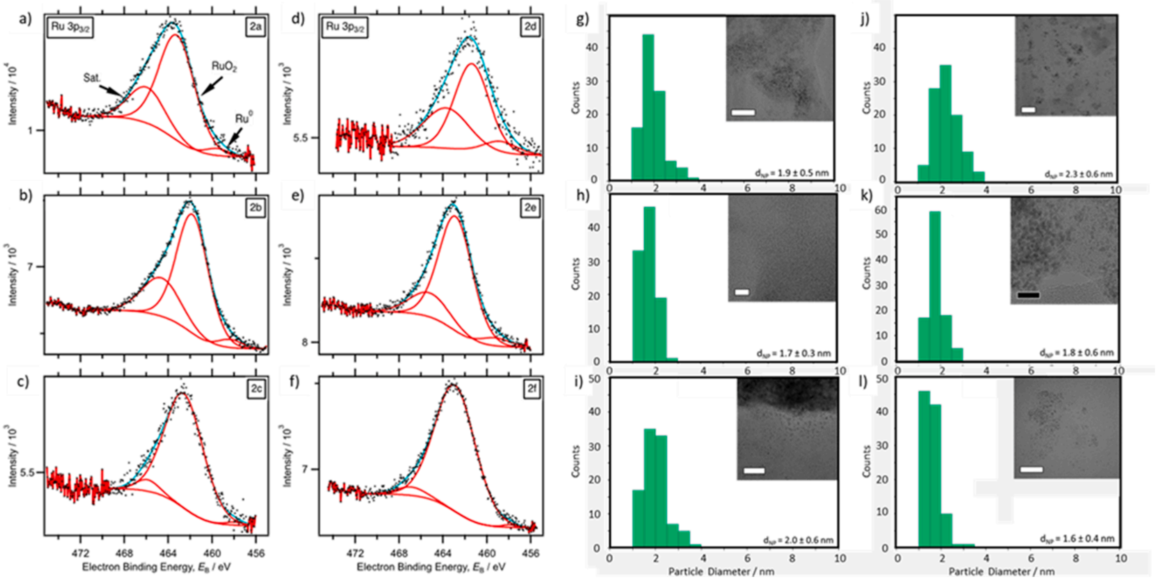

Fig. 2. a-f) XPS data showing the Ru $3p_{3/2}$ region of PIIL-stabilized ruthenium nanoparticles 2a-f respectively and g-l) Sizing data and TEM micrographs (inset) of PIIL-stabilized ruthenium nanoparticles 2a-f. Scale bars are 20 nm (white) and 10 nm (black).

less active with a slightly lower TOF of 117 $mol_{eH2}.mol_{Ru}^{-1}.min^{-1}$. Removal of the amino-group from either of these systems resulted in a reduction in the activity with RuNP@PIILS (**2a**) and RuNP@PEGPIILS (**2b**) giving initial TOFs of 121 $mol_{eH2}.mol_{Ru}^{-1}.min^{-1}$ and 89 $mol_{eH2}.molcat^{-1}.min^{-1}$, respectively. In contrast, under the same conditions, catalysts **2c** and **2d**, stabilised by phosphine oxide-decorated polymer,

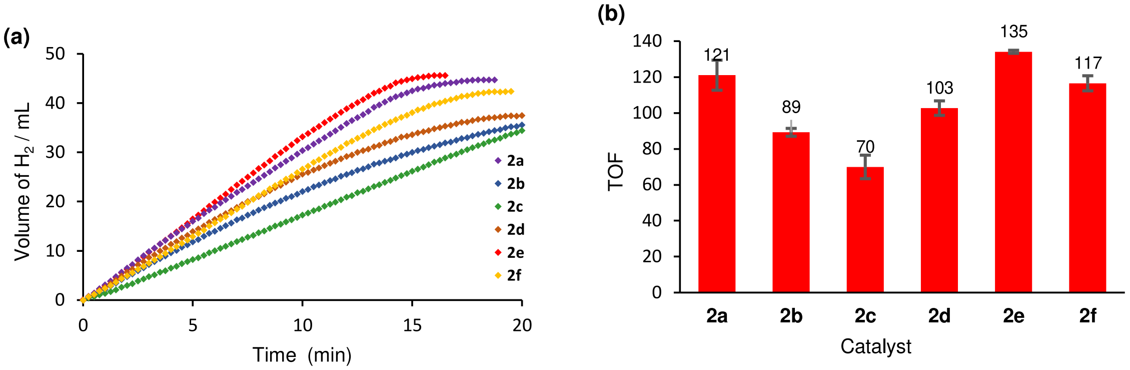

Fig. 3. (a) Hydrolytic release of hydrogen from an aqueous solution of $NaBH_4$ as a function of time at 303 K catalysed by 0.2 mol% 2a-f and (b) corresponding TOFs for the catalytic reactions shown in (a). Conditions: 0.57 mmol $NaBH_4$, 0.2 mol% **2a-f**, water (2 mL), 30°C. Each volume is an average of three runs.

were both less active than their respective amino-modified analogues with initial TOFs of 70 mole$_{H2}$.mol$_{Ru}^{-1}$.min^{-1} and 103 mole$_{H2}$.mol$_{Ru}^{-1}$.min^{-1}, respectively (Fig. 3b). For comparison, 0.16 mol% Ru/C (5 wt%) catalysed this hydrolysis under the same conditions but only reached 57% conversion after 25 min with a TOF of 69 mole$_{H2}$.mol$_{Ru}^{-1}$.min^{-1}. The initial TOF for **2e** improved to 177 mole$_{H2}$.mol$_{Ru}^{-1}$.min^{-1} when the reaction was performed in dilute solution (10 mL) with a reduced catalyst loading of 0.08 mol%. A series of baseline hydrolysis reactions conducted by substituting catalysts **2a-f** with their corresponding polymers **1a-f** confirmed that the RuNPs were essential for catalysis as the gas evolution did not exceed the background reaction under the same conditions.

As there is no clear correlation between the efficacy of catalysts **2a-f** and the nanoparticle size, further studies will be conducted to explore the surface electron density of the RuNPs as a function of the support and to investigate whether the amine influences the hydrogen bonded surface ensemble responsible for substrate activation or improves the dispersibility of the catalyst in the reaction mixture and thereby access to the active site. To this end, amine-modified supports have previously been reported to improve the performance of nanoparticle catalysts compared with the corresponding unmodified catalyst. For example, ruthenium nanoparticles stabilised within the pores of amine-modified MIL-53 (MIL-53(Al)-NH_2) is a significantly more active catalyst for the dehydrogenation of amine-borane than its unmodified counterpart, MIL (Al)-53; this was attributed to the formation and stabilization of ultrasmall RuNPs [76]. There are also numerous additional reports of the beneficial effect on catalyst performance of incorporating an amine onto the surface of a support. For instance, a marked improvement in the activity and selectivity of platinum nanowires for the partial hydrogenation of nitroarenes to *N*-phenylhydroxylamine [126–127], an enhancement in the activity of RuNPs for the hydrogenation of levulinic acid to γ-valerolactone [128], an improvement in activity for the transfer hydrogenation of nitroarenes catalysed by RuNP confined in an amine-modified porous organic polymer [129], an increase in activity for the PtNP-catalysed hydrogenation of quinoline [130], improvements in activity and selectivity for the Pt/Co and PdNP catalysed semi-hydrogenation of alkynes [131–133], and highly selective reduction of the carbonyl in cinnamaldehyde with MOF-confined Pt nanoclusters [134].

Although a comparison of the efficacy of **2a-f** with literature reports of other supported ruthenium nanoparticles should be treated with caution because of the vastly disparate experimental conditions and protocols employed to collect data, the initial TOF of 177 mole$_{H2}$.mol$_{Ru}^{-1}$.min^{-1} is higher than that of 80 mole$_{H2}$.molcat^{-1}.min^{-1} obtained with PEGylated click dendrimer-stabilised RuNPs [78], and 105 mole$_{H2}$.mol$_{Ru}^{-1}$.min^{-1} with ruthenium electrodeposited on nickel foam [135] and a marked improvement on 67 mole$_{H2}$.mol$_{Ru}^{-1}$.min^{-1} obtained in 5% wt NaOH with RuNPs nanoclusters stabilised by confinement in the framework of Zeolite-Y [64], 25 mole$_{H2}$.mol$_{Ru}^{-1}$.min^{-1} for RuNP@ZIF-67 [77] and 35 mole$_{H2}$.mol$_{Ru}^{-1}$.min^{-1} for carbon-supported bimetallic RuCo nanoparticles [136]; but lower than that of 550 mole$_{H2}$.mol$_{Ru}^{-1}$.min^{-1} obtained with RuNPs stabilised in Zeolite-Y [64] and 505 mole$_{H2}$.mol$_{Ru}^{-1}$.min^{-1} with nanoporous ruthenium prepared by chemical dealloying RuAl [137]; to the best of our knowledge these latter systems are the most active ruthenium-based catalysts for this hydrolysis.

As the highest TOF was obtained with **2e**, a thorough study of the reaction kinetics together with deuterium isotope effects, recycle experiments and a tandem reaction using the liberated hydrogen for the tandem hydrogenation of 1,1-diphenylethene with deuterium labelling was undertaken, details of which are discussed herein; for comparison, full details of the corresponding experiments with catalysts **2a-d** and **2f** are provided in the supporting information and discussed in context where appropriate. There have been numerous reports of an enhancement in activity for the metal nanoparticle catalysed hydrolytic evolution of hydrogen from sodium borohydride and amine borane in the presence of added base. For example, Astruc has reported a marked increase in the initial TOF for the hydrolysis of $NaBH_4$ catalysed by click dendrimer-supported RuNPs from 80 mole$_{H2}$.mol$_{Ru}^{-1}$.min^{-1} to 186 mole$_{H2}$.mol$_{Ru}^{-1}$.min^{-1} in the presence of 0.2 M NaOH; an increase in TOF was also observed for a host of other catalysts including Rh, Au, Pd, Co, Ni, Fe and Co nanoparticles with the exception of PtNPs which experienced a strong negative effect [78]. Significant enhancements in TOF were also obtained for the hydrolysis of hydrogen-rich boron compounds with MNP@ZIF-8 (M = Ni, Co), NiPtNP@ZIF-8 and CoPtNP@-dendrimer nanocatalysts in the presence of NaOH [72,73,75,80]. This enhancement has been attributed to coordination of the hydroxide to the nanoparticle surface which increases the electron density and facilitates activation of the O-H bond; in contrast, Pt is an electron-rich metal and highly reactive towards oxidative addition and as such the hydroxide ions occupy surface active sites and prevent substrate coordination. Such a large enhancement in activity for a dendrimer-stabilised RuNP-based catalyst prompted us to study the efficiency of **2a** for the catalytic hydrolysis of $NaBH_4$ as a function of the concentration of sodium hydroxide; reactions were conducted using 0.26 mol% of **2a** to catalyse the hydrolysis of alkaline solutions of 0.28 M $NaBH_4$ with sodium hydroxide concentrations ranging between 0.035 mM to 100 mM (Fig. 4). There was no apparent variation in the initial TOF at low concentrations of NaOH ($<$ 0.035 mM) while the TOFs decreased gradually at concentrations above 0.07 mM; this decrease became more dramatic when the sodium hydroxide concentration reached 5 mM and the initial TOF eventually dropped from 136 mole$_{H2}$.mol$_{Ru}^{-1}$.min^{-1} in the absence of sodium hydroxide to 39 mole$_{H2}$.mol$_{Ru}^{-1}$.min^{-1} in a 100 mM NaOH solution of $NaBH_4$. To this end, there have been several reports of a decrease in the hydrogen generation activity with increasing NaOH concentration (1-10 wt% NaOH) for the ruthenium-catalysed hydrolysis of $NaBH_4$ [138–142], which were attributed to strong interactions between the hydroxide ions and water decreasing the available free water needed for the hydrolysis of $NaBH_4$ [138]. However, it is interesting to note that

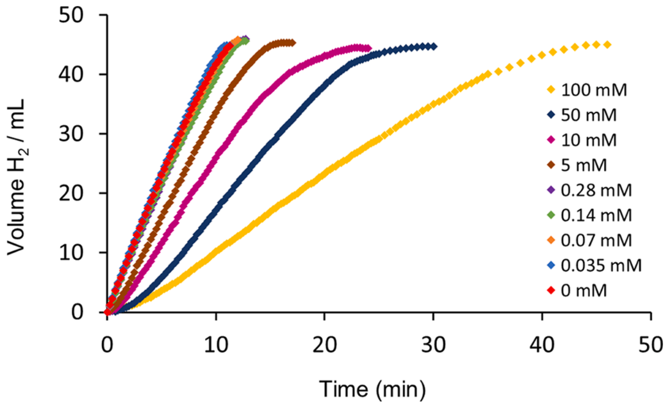

Fig. 4. (a) Volume of hydrogen generated against time for the hydrolysis of 2 mL of alkaline 0.28 M $NaBH_4$ as a function of the sodium hydroxide concentration (0.035 mM - 100 mM) catalysed by 0.26 mol% **2a**. *Conditions*: 0.57 mmol $NaBH_4$ (0.021 g), 0.26 mol% **2a** (0.0025 g), water (2 mL), 303 K. Each volume is an average of three runs.

high concentrations of NaOH have been shown to enhance the hydrogen generation activity for the non-noble metal catalysed hydrolysis of $NaBH_4$, *i.e.* these systems tolerate high concentrations of hydroxide and coordination of the OH^- to the surface does not appear to prevent substate binding [143–148]. As the decrease in hydrogen generation rate for **2a** at a NaOH concentration as low as 0.001 wt% (0.28 mM) is unlikely to be due to a reduction in the activity of water, as described by Amendola, the high rate obtained in the absence of NaOH may reflect the intrinsic activity of ruthenium to facilitate oxidative addition as a late transition metal while the reduction in activity in the presence of even a minor amount of sodium hydroxide (NaOH:catalyst between 0.05:1 and 0.4:1) may be attributed to the hydroxyphilic nature of ruthenium with the hydroxide ions occupying surface active sites and preventing substrate coordination and activation, as described above; even at these concentrations there would be sufficient OH^- ions to populate the surface of the nanoparticle and disrupt the strongly hydrogen bonded $NaBH_4$—H_2O ensemble involved in the rate limiting O-H bond activation step (*vide infra*).

Kinetic studies were subsequently undertaken to determine the temperature dependence of the rate and obtain activation parameters for the hydrolytic release of hydrogen from $NaBH_4$ for a comparison with related systems reported in the literature. A set of reactions were conducted to monitor the hydrolysis of a 0.28 M solution of $NaBH_4$ as a function of time to determine the initial rates across a range of temperatures from 294 K to 313 K. The apparent activation energies (Ea) for the hydrolysis catalysed by **2a-f,** determined from an Arrhenius plot of ln*k* against 1/T (ln*k* = lnA - Ea/RT) using the initial rates calculated from the linear slope of the graph, ranged from 38.9 kJ mol^{-1} to 51.8 kJ mol^{-1} (Fig. 5a-b and Fig. S1 in the supporting information). These values lie within the range reported for the hydrolysis of $NaBH_4$ with other RuNP catalysts including 35 kJ mol^{-1} for RuNPs stabilised in the framework of Zeolite-Y [64], 41 kJ mol^{-1} for water-dispersible, acetate-stabilized RuNPs [149], 36 kJ mol^{-1} for RuNPs confined in ZIF-67 [77], 47 kJ mol^{-1} for RuNPs immobilised by the anion exchange resin IRA-400 [150] and 41.8 kJ mol^{-1} for ruthenium immobilised on Al_2O_3 pellets [151], but slightly lower than 61.1 kJ mol^{-1} for RuNPs supported on amine-modified graphite [139], 56.0 kJ mol^{-1} for RuNP@IRA-400 [138], 58.2 kJ mol^{-1} for $Ru(acac)_3$ [152] and 66.9 kJ mol^{-1} for ruthenium supported on carbon [153]. There does not appear to be a correlation between the activation energies and the initial rates which may be attributed to variations in the number of active sites or their availability as this determines the pre-exponential factor (A) [76, 154].

The hydrogen release was next investigated as a function of the concentration of **2e** across a range of catalyst loadings from 0.12 mol% to 0.28 mol% in 0.28 M $NaBH_4$ (Fig. 6a) and the logarithmic plot of the initial hydrogen generation rate versus catalyst concentration gave a straight line with a slope of 1.04 (Fig. 6b), indicating that the hydrolysis of $NaBH_4$ is first order with respect to the catalyst. Similarly, the corresponding slopes for the logarithmic plots obtained with catalyst **2a-d** and **2f** varied between 0.70 and 1.04, which are all consistent with first order kinetics; full details are presented in Fig. S2 in the supporting information. This data is also consistent with recent reports of noble metal nanoparticle-catalysed hydrogen generation from hydrogen-rich boron derivatives including a slope of 0.73 for RuNPs confined in Zeolite-Y [64], 0.94 for RuNPs stabilized by polyvinylpyrrolidinone [155], 1.06 for $Ru(acac)_3$ [152], 1.17 for porphyrin-stabilised RuNPs [156], 0.85 for PtCoNP@dendrimer [78], and 0.82 for Ni_2Pt@ZIF-8 [73]. The variation in the rate of hydrolysis of $NaBH_4$ as a function of the substrate concentration was also investigated using catalyst **2e**. As the order of reaction with respect to $NaBH_4$ has been reported to depend on the amount of $NaBH_4$ in solution (i.e. the $NaBH_4$:catalyst ratio), changing from 1 to 0 as the concentration of $NaBH_4$ increases [145], kinetic data was obtained by conducting a series of reactions with 0.026 mmol of catalyst **2e** and varying the initial concentration of $NaBH_4$ from 0.066 mM to 0.52 mM as these amounts correspond to catalyst:hydride ratios between 2:1 and 1:4 (Fig. 7). Such low catalyst/hydride mole ratios were used to avoid the BH_4−induced dynamic saturation of the active sites on the catalyst surface which would give zero order kinetics; under these conditions the surface is not completely covered by $NaBH_4$ and there are active sites. The slope of 1.02 obtained from the logarithm plot of hydrogen generation rate versus concentration of $NaBH_4$ confirms that the hydrolysis is first order in substate, which undergoes rate limiting diffusion on the catalyst surface. Under the same conditions, slopes of 1.02 and 1.01 were also obtained with catalysts **2a** and **2f**, respectively, which are both consistent with first order kinetics; see

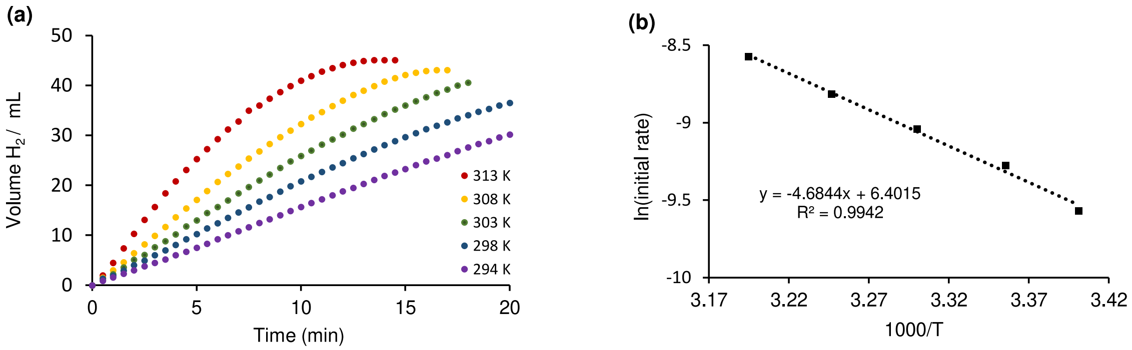

Fig. 5. (a) Plot of volume of hydrogen generated against time for the hydrolysis of 2 mL of 0.28 M $NaBH_4$ across a range of temperatures (temp = 294 K, 298 K, 303 K, 308 K and 313 K) catalysed by 0.16 mol% **2e**; (b) the associated Arrhenius plot for the data in (a); the initial rates were calculated from the slopes of the fitted lines. *Conditions*: 0.57 mmol $NaBH_4$ (0.021 g), 0.26 mol% **2a**, 0.32 mol% **2b**, 0.45 mol% **2c**, 0.11 mol% **2d**, 0.16 mol% **2e** and 0.32 mol% **2f** in water (2 mL). Each volume is an average of three runs. Initial rate = $mol_{H2}·min^{-1}$.

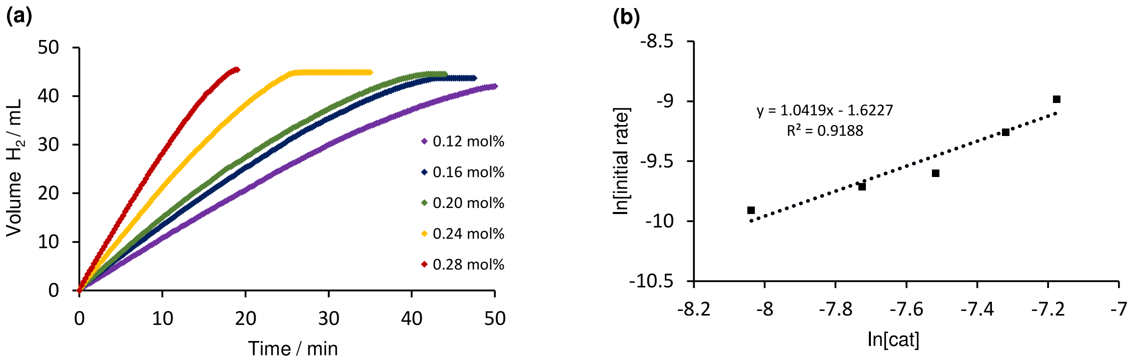

Fig. 6. (a) Plot of volume of hydrogen generated against time for the hydrolysis of 2 mL of 0.28 M $NaBH_4$ catalysed by various amounts of **2e**; (b) corresponding plot of the initial hydrogen generation rate against catalyst concentration in logarithmic scale. *Conditions*: 0.57 mmol $NaBH_4$ (0.021 g), 0.12, 0.16, 0.20, 0.24, 0.28 mol% **2a**, water (2 mL), 298 K. Each volume is an average of three runs. Initial rate = $mol_{H2}\cdot min^{-1}$.

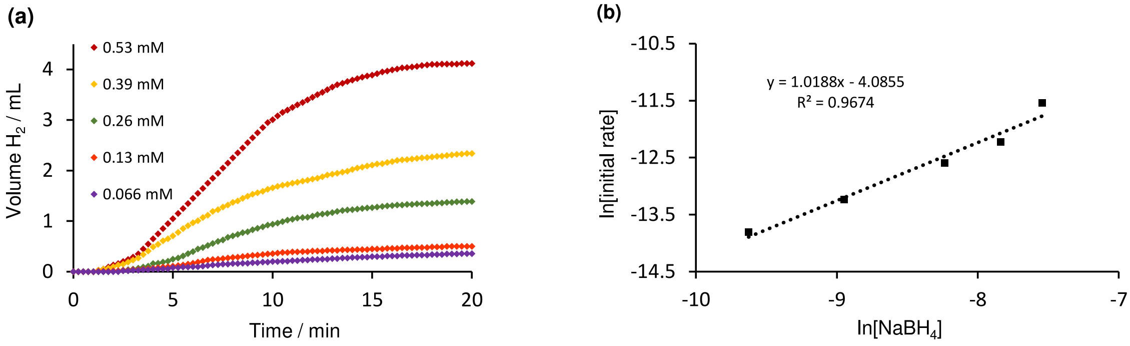

Fig. 7. (a) Plot of volume of hydrogen generated against time for the hydrolytic dehydrogenation of $NaBH_4$ at 298 K catalysed by **2e** (0.026 mmol, 0.0764 g), in water (200 mL), initial concentrations of sodium borohydride ($[NaBH_4]_0$ = 0.066, 0.13, 0.26, 0.39, 0.53 mM); (b) the corresponding plot of the initial hydrogen generation rate against concentration of sodium borohydride in logarithmic scale. Each volume is an average of three runs. Initial rate = $mol_{H2}\cdot min^{-1}$.

Fig. S3 in the electronic supporting information. First order kinetics with respect to $NaBH_4$ have previously been reported for ruthenium on carbon [142], palladium on carbon [157] and Pd and Pt dispersed on functionalised surfaces of carbon nanotubes [158] when reactions were conducted at low concentrations of $NaBH_4$. A similar study conducted with catalyst **2e** at much higher catalyst/hydride mole ratios between 1:625 and 1:2500 gave a slope of 0.26 which is indicative of zero order kinetics due to saturation of the active sites on the catalyst surface during the reaction (Fig. S4 in the supporting information), as described by Patel [145]. A slope of 0.17 was also obtained using catalysts **2d** which is also consistent with zero order kinetics; similar kinetics have previously been described for ruthenium nanoclusters [159], Ru supported on IRA 400 [150] and ruthenium on carbon [153].

3.2. *Kinetic isotope effects*

The kinetic isotope effect (KIE) is a valuable tool for elucidating information about the rate limiting step (RLS) of a reaction that has been routinely used to probe the catalytic hydrogen generation from borohydride and amine borane (AB) [160,72,79,80]. While the reaction kinetics are complicated and the mechanism still not fully understood [42] it is clear that both $NaBH_4$ and ammonia-borane are hydride donors and provide one of the two hydrogen atoms of the derived hydrogen gas while water provides the other in the form of a proton [41,43] and that the rate determining step involves activation of one of the O-H bonds of water, as measured by the large primary KIE obtained when the hydrolysis is performed in D_2O instead of H_2O [78,79,80,83,161,162]. Activation of an O-H bond has been proposed to occur *via* oxidative addition involving a hydrogen-bonded ensemble between a surface-coordinated borohydride and a water proton; the hydrogen could then be liberated either *via* reductive elimination between a borohydride-derived NP-H and the water-derived NP-H (Fig. 8, pathway a-c) or a concerted σ-bond metathesis-like process between a surface coordinated $[BH_4]^-$ and a water-derived NP-H (Fig. 8, pathway d-e), which may be facilitated by hydroxide. Alternatively, the protonic and hydridic hydrogen atoms may be transferred to the nanoparticle surface by oxidative addition of both the O-H and B-H bonds, respectively, to afford a dihydride that would generate hydrogen and BH_3-OH via reductive elimination (Fig. 8, pathway f-g), as proposed by Astruc for the CoNP@ZIF-8 catalysed hydrolysis of $NaBH_4$ [75]. While the pathways described in Fig. 8 are all initiated by oxidative addition of the O-H bond

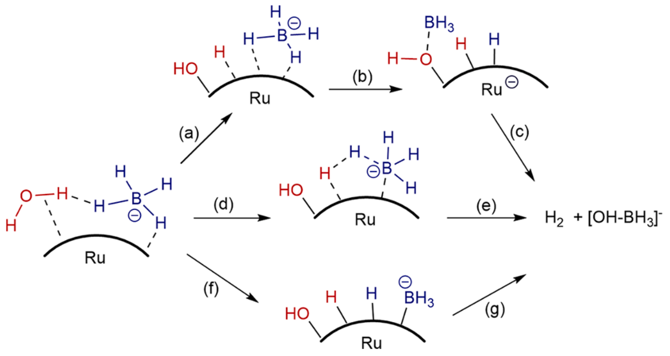

Fig. 8. Proposed pathways for RuNP-catalyzed hydrolytic hydrogen evolution from the hydrogen-bonded surface-coordinated ensemble $[H_3B-H—H-OH]$ via (a-c) oxidative addition of an O-H bond and hydride transfer followed by reductive elimination of H_2 (d-e) oxidative addition of an O-H bond followed by σ-bond metathesis involving the water-derived metal hydride and a surface-coordinated borohydride or (f-g) oxidative addition of the O-H and B-H bonds followed by reductive elimination of H_2 and $[HO-BH_3]^-$.

of water via a hydrogen-bonded ensemble involving a surface-coordinated borohydride, Jagirdar [163] and Ma [164] have suggested that activation of the O-H bond and generation of H_2 could occur via a hydrogen-bonding interaction between a surface adsorbed water and a surface hydride generated via rapid hydride transfer from $NaBH_4$ to the NP surface.

The role of H_2O in the hydrolysis of $NaBH_4$ catalysed by **2e** was explored by conducting the reaction in D_2O and monitoring the hydrogen evolution as a function of time to determine the KIE. Reactions were conducted under the conditions of catalysis *i.e.* 0.16 mol% of **2e** was used to catalyse the hydrolysis of 2 mL of a 0.28 M solution of $NaBH_4$ at 30°C. A comparison of the efficacy of **2e** as a catalyst for the hydrolysis of $NaBH_4$ in H_2O and D_2O revealed that the reaction was more rapid in H_2O than in D_2O with a primary kinetic isotope effect (k_H/k_D) of 2.31 (Fig. 9a); similar values of k_H/k_D were obtained with catalysts **2a** ($k_H/k_D = 1.76$) and **2d** ($k_H/k_D = 1.53$) and the corresponding data is presented in Fig. S5a-b in the supporting information. This value is comparable to the solvent isotope effect of 2.25 obtained by Astruc for the gold-ruthenium nanoalloy catalysed visible light-accelerated hydrolytic dehydrogenation of $NaBH_4$ and amine-borane [165] as well as 1.8 determined in a detailed kinetic analysis of the platinum-catalysed hydrolysis of $NaBH_4$ in alkaline media [162], 2.3 for dendrimer-stabilised RhNPs [79], 2.4 for PtCo@dendrimer [80] and 2.49 for NiNP@ZIF-8 [72] and supports a mechanism with rate limiting cleavage of an O-H bond of water in a surface-coordinated hydrogen-bonded ensemble of the type described above and shown in Fig. 8. The same comparison of initial rates between reactions conducted in H_2O and D_2O under stoichiometric conditions using 26 μmol of **2e** for the catalytic hydrolysis of 200 mL of a 0.13 mM solution of $NaBH_4$ at 30°C (catalyst:$NaBH_4$ ratio of 1:1) gave a primary kinetic isotope effect of 1.7 (Fig. S6d in the supporting information), which is also consistent with rate limiting oxidative addition of water. However, this KIE does not distinguish between a rate limiting step in which a surface coordinated $NaBH_4$——HOH ensemble activates an O-H bond towards oxidative addition through a hydrogen-bonding interaction to afford a water-derived metal hydride and a surface-coordinated borohydride, such as that shown in Fig. 8 pathway a, and concerted activation of both the B-H and O-H bonds in a similar hydrogen-bonded ensemble; the latter process would most likely occur via oxidative addition of the O-H bond and rapid hydride transfer from the borohydride (Fig. 8 pathway a-c) rather than oxidative addition of both the O-H and B-H bonds (Fig. 8, pathway f-g) as borohydrides are extremely potent transfer reagents. For the same reason, a subsequent σ-bond metathesis involving the surface-coordinated borohydride and the water-derived RuNP hydride would also be unlikely (Fig. 8, pathway e).

Thus, the mechanism was further probed by comparing the rates of hydrolysis of $NaBD_4$ and $NaBH_4$ catalysed by **2e** at 30°C. Analysis of the initial rates obtained for the hydrolysis of 200 mL of a 0.13 mM solution of $NaBH_4$ and $NaBD_4$ catalysed by 26 μmol of **2e**, i.e., a substrate/catalyst ratio of 1, gave a primary kinetic isotope effect (k_H/k_D) of 2.72 (Fig. 9b). Reassuringly, comparable values were also obtained with catalysts **2a** ($k_H/k_D = 2.25$) and **2d** ($k_H/k_D = 2.37$), full details of which are presented in Fig. S6a-b in the supporting information. These values are comparable to that of 2.2 obtained for the visible light-accelerated H_2 evolution from $NaBH_4$ catalysed by a gold-ruthenium nanoalloy; which, together with a KIE of 2.5 obtained for the hydrolysis of $NaBH_4$ in D_2O, was taken to indicate that both the O-H and B-H bonds were activated by the ruthenium atoms in the rate limiting step, most likely via concerted oxidative addition-hydride transfer, involving the surface-coordinated hydrogen-bonded $[BH_3H^-]$——H-OH ensemble, rather than oxidative addition of both the O-H and B-H bonds [75,165]. Interestingly though, comparison of the rates obtained under the conditions of catalysis using **2e** to catalyse the hydrolysis of 2 mL of 0.28 M solutions of $NaBH_4$ and $NaBD_4$ at 30°C gave a KIE of 0.65 (Fig. 9c); similar values were also obtained with catalysts **2a** ($k_H/k_D = 0.87$) and **2d** ($k_H/k_D = 0.85$), full details of which are provided in Fig. S5d-f in the supporting information. These are inverse kinetic isotope effects and would be consistent with a surface-coordinated borohydride activating an O-H bond of water in the hydrogen-bonded ensemble prior to hydride transfer.

3.3. *Tandem hydrogenation and deuterium labelling studies*

The hydrogen liberated from the catalytic hydrolysis of $NaBH_4$ was used for the hydrogenation of 1,1-diphenylethene with various labelling experiments to determine the fate of the liberated hydrogen. In the first of these, the tandem reaction was conducted using 0.26 mol% **2a** to generate hydrogen from a 0.28 M solution of $NaBH_4$ in D_2O at 30°C in a sealed tube; after 70 min the connector was opened to the second flask which contained 1,1-diphenylethene and 0.5 mol% Pd/C in d_4-methanol and the resulting mixture was stirred for 18 h. Interestingly, analysis of the crude mixture by ^1H, ^2H and ^{13}C NMR spectroscopy and mass spectrometry revealed that a mixture of all eight isotopologues of 1,1-diphenylethane had been generated (Scheme 1). Analysis of the methine region (δ 44.5 ppm) of the $^{13}C\{^1H\}$ NMR spectrum was used to identify and assign each of the isotopologues, which appear as a set of four singlets at δ 44.88, 44.81, 44.73, and 44.66 ppm corresponding to **I, II, III**, and **IV**, respectively, while **V, VI, VII** and **VIII** appear as a set of four 1:1:1 triplets at δ 44.46, 44.39, 44.31 and 44.24 ppm, respectively, resulting from a J_{CD} of 19.5 Hz due to the deuterium atom attached to the methine carbon; the methyl group of these isotopologues has either zero, one, two, or three deuterium atoms. The experimental spectrum of the reaction mixture and the summed simulated spectrum of each isotopologue are shown in Fig. 10 (see Fig. S71 in the supporting information for full details of the simulated spectrum for each isotopologue). The summed simulated spectrum is remarkably similar to the

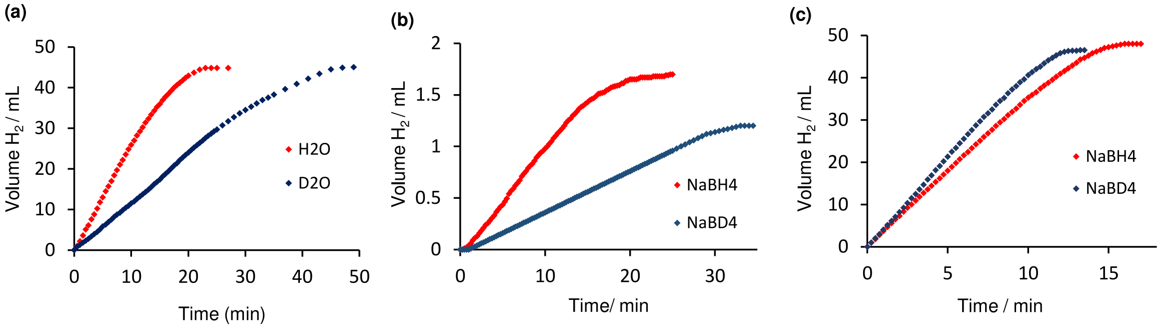

Fig. 9. (a) Hydrogen release from 2 mL of 0.28 M $NaBH_4$ in H_2O (red line) and D_2O (blue line) at 303 K, catalysed by 0.16 mol% **2e** (0.0025 g) (b) hydrogen release from 200 mL of 0.13 mM solutions of $NaBH_4$ (red line) and $NaBD_4$ (blue line) in H_2O at 303 K using a stoichiometric amount of catalyst **2e** (0.026 mmol, 0.0764 g); (c) hydrogen release from 2 mL of a 0.28 M solution of $NaBH_4$ (red line) and $NaBD_4$ (blue line) in H_2O at 303 K catalysed by 0.2 mol% **2e** (0.0033 g) Each volume is an average of three runs.

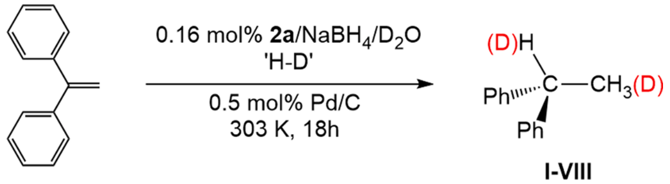

I-VIII

Scheme 1. The distribution of isotopologues **I-VIII** obtained from the hydrogenation of 1,1-diphenylethene in d_4-MeOH using HD generated from the catalytic hydrolysis of $NaBH_4$ in D_2O using 0.16 mol% **2e.** Relative proportions: (**I**) Ph_2CHCH_3 (22.9%), (**II**) Ph_2CHCH_2D (25.9%), (**III**) Ph_2CHCD_2H (13.8%), (**IV**) Ph_2CHCD_3 (4.5%), (**V**) Ph_2CDCH_3 (13.2%), (**VI**) Ph_2CDCH_2D (10.7%), (**VII**) Ph_2CDCHD_2 (6.7%), (**VIII**) Ph_2CDCD_3 (2.4%).

experimental spectrum, which supports the assignment of the isotopologues and their relative proportions and confirms that the coupling constants, chemical shifts and line intensities and widths have been correctly determined. On the basis that the hydrogen generated from the hydrolysis of $NaBH_4$ in D_2O should result from a water-derived proton and a borohydride-derived hydride, the deuterium incorporation for all isotopologues **II-VIII** should be one. To this end, the total deuterium incorporation of 1.3 is slightly higher than expected and could be due to H/D exchange either with the d_4-MeOH on the Pd/C during the hydrogenation or from the generation of a mixture of HD and D_2 by exchange at the NP surface after O-D bond activation. A complementary experiment using hydrogen liberated from $NaBH_4/H_2O$ for the hydrogenation of 1,1-diphenylethene in d_4-methanol gave a total deuterium incorporation of 0.3, which confirms that H/D exchange occurs on the surface of the Pd/C; moreover, this deuterium incorporation corresponds to the excess of 0.3 above the total deuterium incorporation of one that was expected when the hydrogenation was performed in d_4-MeOH with hydrogen generated from $NaBH_4/D_2O$. The hydrogenation was also performed in toluene with hydrogen generated from $NaBH_4$ in D_2O to investigate exchange at the NP surface. Under these conditions, the total deuterium incorporation of 0.93 was close to one, indicating that H/D exchange at the NP surface is slow; a total deuterium incorporation of 1.76 was also obtained when the hydrogenation was performed in toluene using hydrogen generated from $NaBD_4$ in D_2O, which is reassuringly close to the predicted value of two. Finally, the generation of minor amount of isotopologues containing $-CHD_2$ and $-CD_3$ (**III, IV, VII** and **VIII**) from each of these deuterium labelling experiments is consistent with H/D scrambling via facile reversible β-hydride elimination from a surface $M\text{-}CPh_2CH_2D$ species, reinsertion of the resulting $Ph_2C{=}CHD$ into a surface M-D followed by reductive elimination from $(D)HPd\text{-}CPh_2CH_{3\text{-}n}D_n$ ($n = 2, 3$); full details of the relative proportions of each isotopologue obtained from these labelling studies are summarised in the supporting information. A higher than stoichiometric incorporation of deuterium recently reported for the hydrogenation of styrene using 'HD' generated from the hydrolysis of tetrahydroxydiboron with D_2O using quantum dot stabilised PtNPs was also attributed to facile reversible alkene insertion-extrusion involving metal-hydride/deuteride species [166].

3.4. *Catalyst recycle and poisoning studies*

Recycle studies were conducted with 2 mol% loading of **2e** to investigate its activity profile during reuse and thereby its stability and longevity and potential for use in a scale-up system. The practical issues associated with separating and recovering a small amount of catalyst by filtration without loss of material after each run meant that it was not possible to perform a conventional recycle experiment. As such, a reuse experiment was undertaken by monitoring the hydrolysis until gas evolution was complete, the aqueous reaction mixture was then charged with a further portion of $NaBH_4$ and the gas evolution monitored; this sequence was repeated to map the catalyst efficacy against reaction time and reuse number. While the comparative conversions and TOFs shown in Fig. 11a, b were obtained during the first 2 min of the hydrolysis to enable a meaningful comparison between runs, complete conversions were obtained for each run within 4 min. The resulting gas evolution-time profile and corresponding conversion-cycle number profile in

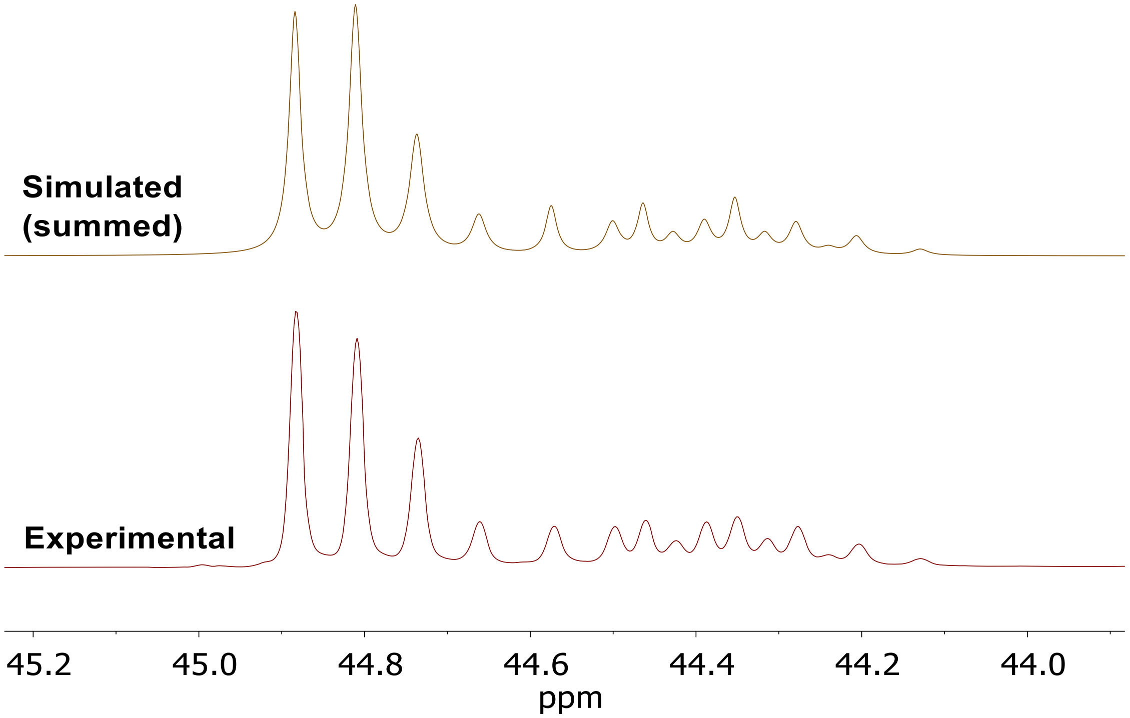

Fig. 10. Plots of the methine region of the experimental $^{13}C\{^1H\}$ NMR spectrum and summed simulated $^{13}C\{^1H\}$ NMR spectrum for the eight isotopologues generated from the hydrogenation of 1,1-diphenylethene in d_4-methanol using hydrogen generated from the catalytic hydrolysis of $NaBH_4$ in D_2O using 0.16 mol % **2e**.

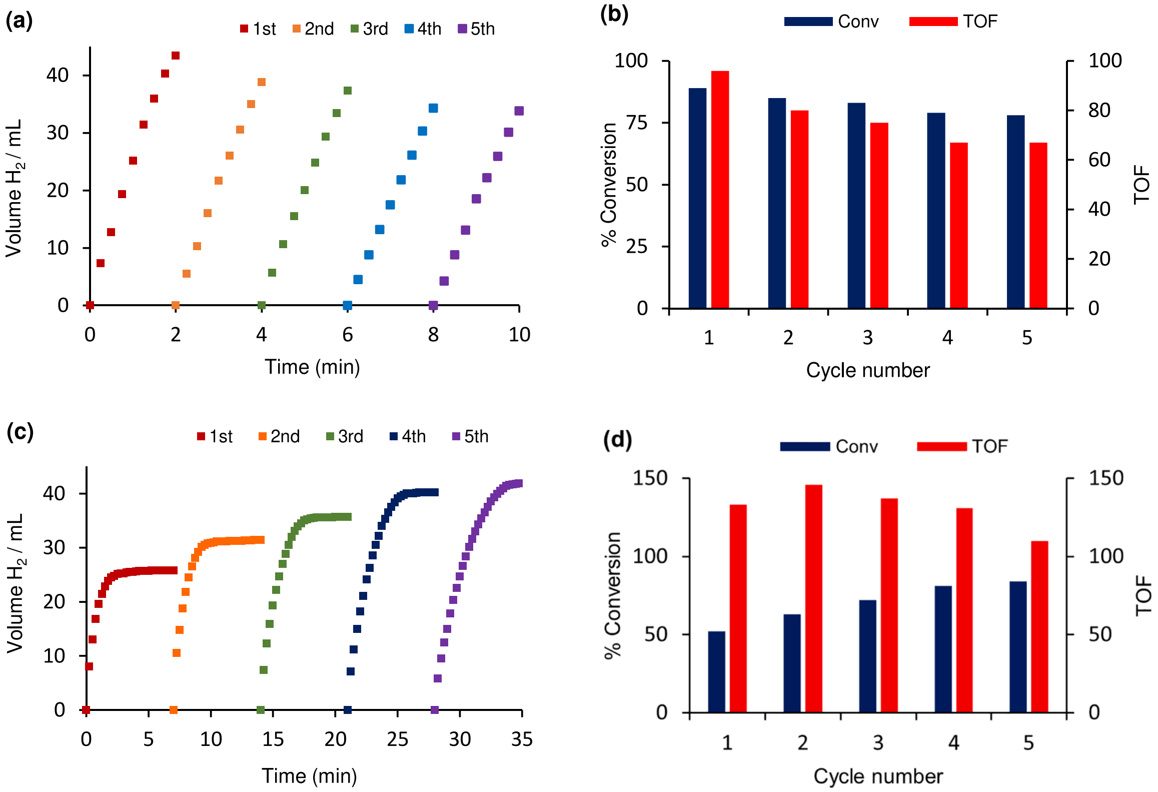

Fig. 11. (a) Reusability study showing plots of volume versus time for the hydrolysis of 20 mL of a 0.028 M solution of $NaBH_4$ catalysed by 2 mol% **2e** across five runs; (b) conversion reached in each run (blue) and initial TOF in $mole_{H2}.mol_{Ru}^{-1}.min^{-1}$ for each run (red). *Conditions*: 0.57 mmol $NaBH_4$ (0.021 g), 2 mol% **2e** (0.0335 g, 0.0114 mmol), water (20 mL), 303 K. Each volume is an average of three runs. (c) Reusability study showing plots of volume versus time for the hydrolysis of 20 mL of a 0.028 M aqueous borate-buffered solution of $NaBH_4$ catalysed by 1 mol% **2e** across five runs; (d) conversion reached in each run (blue) and initial TOF in $mole_{H2}.mol_{Ru}^{-1}.min^{-1}$ for each run (red). *Conditions*: 0.57 mmol $NaBH_4$ (0.021 g), 1 mol% **2e** (0.0165 g, 0.0056 mmol), aqueous borate buffer solution (20 mL), 303 K. Each volume is an average of three runs.

Fig. 11a, b shows a minor but gradual drop in conversion across five reuses, from 89% after 2 min in the first run to 78% after the same time in the 5th run. The drop in catalyst activity in successive runs, defined as the percentage reduction in the initial TOF, shows that **2e** retains 71% of its activity across five reuses (Fig. 11b, red); this is comparable to recycle studies reported for other noble metal nanoparticle catalysts including; RuNPs immobilised in ZIF-67 [77], PtCoNPs supported on carbon nanospheres [167], ruthenium nanoparticles immobilised within the pores of amine-functionalised MIL-53 [76], ruthenium supported on graphite [139], RuCo nanoclusters incorporated in PEDOT/PSS polymer [168], RuNP stabilized by polyvinylpyrrolidone, zeolite-confined RuNPs [64], click dendrimer-stabilized PtCo, Rh and Pt nanoparticles and gold-transition metal nanoalloys [72,73,78,79,80,165] and Ru-RuO_2/C [141].

Sneddon et al. previously reported that the use of a borate buffered solution for the rhodium-catalysed release of hydrogen from ammonia triborane extended the catalyst lifetime such that Rh/Al_2O_3 showed little change in the hydrogen release rate over 11 cycles [169]. Following this lead, a preliminary comparative recycle hydrolysis conducted in freshly prepared aqueous borate buffer (pH maintained between 7.2 and 8) containing 0.28 M $NaBH_4$ and 1 mol% **2e** resulted in a marked increase in activity as evidenced by the initial TOF of 133 $mole_{H2}.mol_{Ru}^{-1}.min^{-1}$ obtained for the first run compared with 95 $mole_{H2}.mol_{Ru}^{-1}.min^{-1}$ for the corresponding reaction in water. The initial TOF increased to 146 $mole_{H2}.mol_{Ru}^{-1}.min^{-1}$ in the second run but then decreased gradually in subsequent cycles to 109 $mole_{H2}.mol_{Ru}^{-1}.min^{-1}$ in the final run (Fig. 11d); even though this represents a 26% reduction in activity over the 5 cycles, it remains higher than the TOFs obtained in water under the same conditions. Interestingly, the data in Fig. 11c, d also shows that the conversion-time profile changes quite dramatically in successive cycles such that the conversion increases from 54% after 5 min in the first run to 80% at the same time interval in the final run; in contrast, for reactions conducted in the absence of buffer, conversions decreased gradually in successive runs (Fig. 11b). A hydrolysis catalysed by 1 mol% **2e** was also conducted in 0.34 M boric acid to provide a benchmark as the borate buffer solution was prepared with this concentration of boric acid and, under otherwise identical conditions, the initial TOF of 66 $mole_{H2}.mol_{Ru}^{-1}.min^{-1}$ was significantly lower than that obtained in the aqueous borate buffer solution (See Fig. S7 in the supporting information). Further studies are currently underway to identify an optimum buffer for this reaction and to develop an understanding of the changes in the conversion-time profile in consecutive runs as well as the origin of the enhancement in activity obtained when the catalysis is conducted in aqueous buffer.

ICP-OES analysis of the aqueous reaction mixture recovered after the fifth run revealed that the ruthenium content was below the detection limit, suggesting that the reduction in activity was unlikely to be due to leaching of the ruthenium to generate a homogeneous species that was less active. Hot filtration studies were also conducted to explore whether soluble ruthenium species might be responsible for the gas evolution. Following a typical protocol, a hydrolysis reaction catalysed by 2 mol% **2e** was filtered through a 45-micron syringe filter at *ca.* 50% conversion. The hydrogen liberated from the filtrate was monitored and corresponded to the background hydrolysis in the absence of catalyst (Fig. 12, blue line), indicating that the active species had been removed in the filtration *i.e.* it is heterogeneous, and that leaching does not generate active soluble ruthenium species. In a complementary hot filtration study a catalytic hydrolysis that reached completion was filtered through a syringe filter (0.45 μm) and a fresh portion of $NaBH_4$ added to the filtrate. The hydrogen liberated also corresponded to the

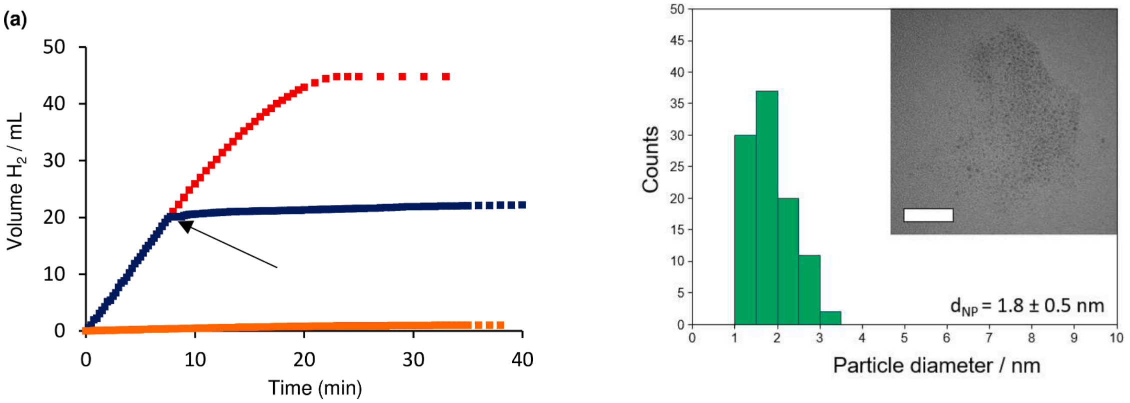

Fig. 12. (a) Hot filtration experiment for the hydrolysis of 20 mL of a 0.028 M solution of $NaBH_4$ at 303 K catalysed by 0.16 mol% **2e** (0.0026 g), confirming that filtration quenches the reaction. Red line – hydrogen evolution in the presence of **2e**; blue line – hydrogen evolution in the presence of catalyst with filtration at t = 7.75 min; orange line – hydrogen evolution after filtration at complete conversion and addition of a further portion of $NaBH_4$; (b) sizing histogram of RuNPs for **2e** after five reuses and a TEM image of the recovered material, scale bar = 20 nm.

uncatalyzed hydrolysis providing further support that the active species is heterogeneous (Fig. 12, orange line). TEM analysis of the catalyst isolated after the fifth run revealed that the ruthenium nanoparticles remained essentially monodisperse with a mean diameter of 1.8 ± 0.5 nm compared with 1.8 ± 0.6 nm for the freshly prepared catalyst (Fig. 12b) which suggests that agglomeration is not responsible for the drop in conversion with increasing use.

There have been several reports that the sodium metaborate tetrahydrate by-product generated during the hydrolysis of $NaBH_4$ deactivates the catalyst by adsorption on the surface [67,71,76,80,135, 170-172], although Wie has demonstrated that the activity of deactivated Ru on nickel foam catalyst can be partially replenished by washing the catalyst with deionised water and completely replenished by washing with HCl to remove the $NaBO_2$ [135]. As such, a series of poisoning studies were undertaken to examine the influence of the by-product on catalyst performance; this involved pre-stirring an aqueous suspension of **2e** with 100 equivalents of sodium metaborate prior to addition of $NaBH_4$ and monitoring the progress of the reaction as a function of the pre-stirring time. A ^{11}B NMR spectrum of a typical reaction solution confirmed that the tetrahydroxyborate anion $B(OH)_4$ was the sole by-product as the spectrum contained a single sharp resonance at δ 2.2 ppm [162,173]; no other species such as partially hydrolysed intermediates were detected. A comparison of the hydrogen evolution in the absence of $NaBO_2$ against the corresponding reaction with added $NaBO_2$ as a function of the pre-stirring time (Fig. 13a,b) confirms that the addition of metaborate passivates the catalyst. The conversions obtained after a reaction time of 2 min and the corresponding initial TOFs as a function of pre-stirring time reveal that the passivation is instantaneous as the TOF drops from 84 $mole_{H2}.mol_{Ru}^{-1}.min^{-1}$ in the absence of $NaBO_2$ to 80 $mole_{H2}.mol_{Ru}^{-1}.min^{-1}$ immediately after the addition of the $NaBO_2$ with no pre-stirring (time = 0 min); the TOFs continue to drop gradually to 57 $mole_{H2}.mol_{Ru}^{-1}.min^{-1}$ as the pre-stirring time was increased to 60 min.

Finally, the formation of $NaBO_2$ can also be monitored by measuring the pH of the reaction solution as a function of time for the catalytic hydrolysis of a 0.028 M solution of $NaBH_4$ using 2 mol% of **2e.** Fig. 14 shows that the pH of the reaction solution clearly maps to the conversion with a gradual increase from pH 8.3 at time = 0 min, recorded immediately after addition of the $NaBH_4$, to pH = 11.1 after *ca.* 2.5 min when the gas evolution had finished; for comparison a 0.028 M solution of $NaBO_2$ in the absence of catalyst or $NaBH_4$ has a pH of 11.30, which correlates with the pH of a hydrolysis reaction at high conversion.

4. Conclusions

Ruthenium nanoparticles stabilized by polymer immobilized ionic liquids catalyze the hydrolytic evolution of hydrogen from sodium borohydride; catalyst stabilized by an amino-modified imidazolium-based polymer was the most active with an initial TOF of 171 $mole_{H2}.mol_{Ru}^{-1}.min^{-1}$, this is among the highest to be reported for a RuNP-based system. Kinetic studies revealed that the reaction was first order in catalyst as well as sodium borohydride at low hydride/catalyst mole ratios but zero order with respect to $NaBH_4$ concentration with high hydride/catalyst mole ratios. The apparent activation energies of 38.9

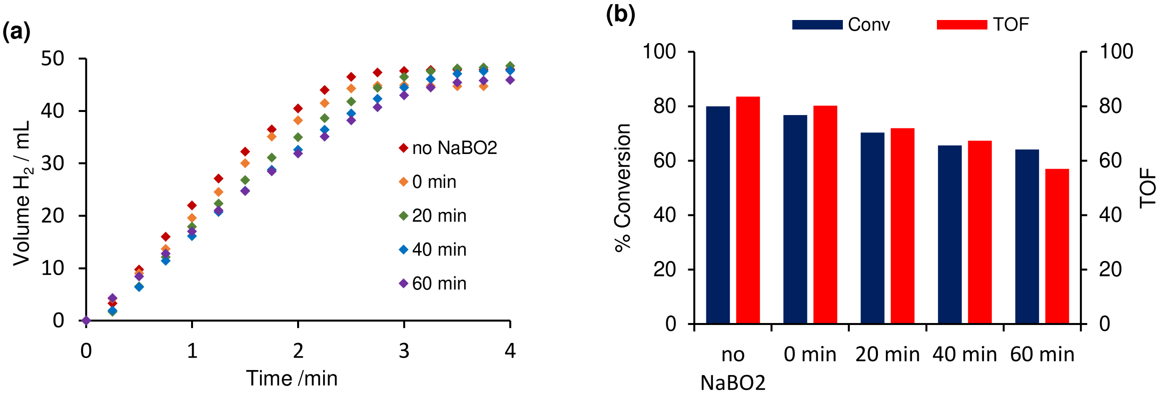

Fig. 13. (a) Volume of hydrogen against time for the hydrolysis of 20 mL of a 0.028 M solution of $NaBH_4$ at 303 K catalysed by 2 mol% **2e** (0.0335 g, 0.0114 mmol) as a function of pre-stirring time with added $NaBO_2$ (0.0765 g, 0.57 mmol); (b) conversions obtained after a reaction time of 2 min and the corresponding initial TOFs as a function of pre-stirring time with $NaBO_2$.

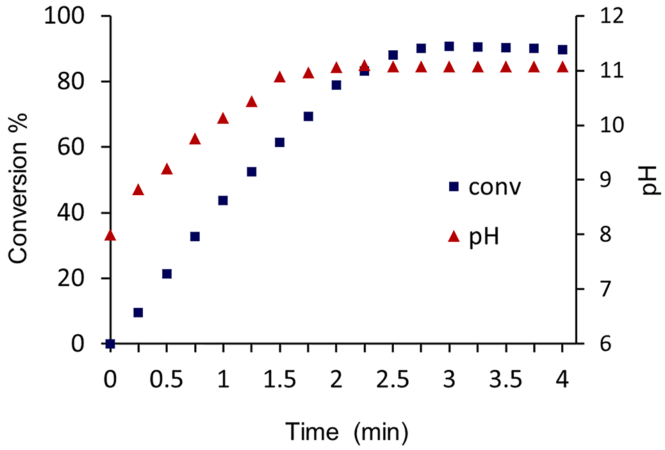

Fig. 14. A plot of pH and conversion against time for the hydrolysis of a 0.028 M solution of $NaBH_4$ (20 mL) at 303 K catalysed by 2 mol% 2e (0.0335 g).

kJ mol^{-1} to 51.8 kJ mol^{-1} are in the region commonly reported for the platinum group metal catalyzed hydrolysis of hydrogen rich boron derivatives; the apparent activation energy of 38.9 kJ mol^{-1} for RuNP@NH_2PIILS is lower than each of the other catalysts tested and consistent with its higher initial TOF. A kinetic isotope effect (k_H/k_D) of 2.3 obtained for reactions conducted in H_2O and D_2O and a k_H/k_D of 2.72 for reactions conducted with $NaBH_4$ and $NaBD_4$ at a low catalyst/hydride mole ratio indicate that both the O-H and B-H bonds are activated by the ruthenium atoms in the rate limiting step, most likely via a concerted oxidative addition-hydride transfer involving the surface-coordinated hydrogen-bonded [BH_3H-]——H-OH ensemble rather than oxidative addition of both the O-H and B-H bonds. Interestingly though, the k_H/k_D of 0.67 obtained from comparing the initial rates of hydrolysis for $NaBH_4$ and $NaBD_4$ under conditions of catalysis, *i.e.* at a high catalyst/hydride mole ratio, is an inverse KIE which would be consistent with a surface-coordinated borohydride activating an O-H bond of water in the hydrogen-bonded ensemble prior to rapid hydride transfer. Reuse experiments showed that RuNP@NH_2-PIILS retains 79% of its activity over 5 runs and poisoning studies conducted by adding $NaBO_2$ to a catalytic reaction suggest that the reduction in activity is most likely due to passivation of the catalyst by absorption of the metaborate by-product on the nanoparticle surface. A tandem hydrogenation of 1,1-diphenylethene in d_4-MeOH with hydrogen generated from the catalytic hydrolysis of $NaBH_4$ in D_2O gave a mixture of all eight possible isotopologues with a total deuterium incorporation greater than one while the use of toluene for the hydrogenation using $NaBH_4/D_2O$ gave a total deuterium incorporation close to one. This is consistent with slow H/D exchange at the NP surface and fast H/D exchange on the surface of the Pd/C coupled with H/D scrambling via facile reversible beta hydride elimination-reinsertion during the hydrogenation. This programme is currently exploring the use of PIIL supported bimetallic nanoparticles with varying proportions of noble and earth abundant metals to establish how the composition of the NP influences catalyst performance with the aim of identifying an optimum synergism that will be suitable for use as a hydrogen generation system for portable applications of proton exchange membrane fuel cells (PEMFC). In addition, PIILs are an ideal support to investigate how polymer properties such as charge density, the number and type of heteroatom donor and functionality, porosity and hydrophilicity influences the size, morphology, and efficacy of the nanoparticles as well as to tailor catalyst-support interactions to enhance efficacy. Ultimately, this catalyst technology will be extended to include the hydrogen evolution reaction to develop stable, durable, highly active cost-effective catalysts for use in AEM based electrolysers and fuel cells.

Declaration of Competing Interest

The authors declare the following financial interests/personal relationships which may be considered as potential competing interests: Reece Patterson, Anthony Griffiths reports financial support was provided by Engineering and Physical Sciences Research Council.

Data availability

Data will be made available on request.

Acknowledgments

R.P. gratefully acknowledges the Engineering and Physical Sciences Centre for Doctoral Training in Renewable Energy Northeast Universities (‘ReNU’) EP/S023836/1 for a studentship and A.A. thanks Taibah University, Saudi Arabia for a Scholarship. We also thank (Dr Tracey Davey) for the SEM images (Faculty of Medical Sciences, Newcastle University) and Zabeada Aslam and the Leeds electron microscopy and spectroscopy centre (LEMAS) at the University of Leeds for TEM analysis. This research was funded through a studentship (Anthony Griffiths) awarded by the Engineering and Physical Sciences Centre for Doctoral Training in Molecules to Product (EP/SO22473/1). The authors greatly acknowledge their support of this work. This article is dedicated to the memory of Professor Stephen A. Westcott (Canada Research Chair holder in the Department of Chemistry & Biochemistry, Mount Allison University, Canada) who recently passed away; a fantastic scientist, a great ambassador for chemistry teaching and research in Canada and across the globe, a generous, genuine and kind human being but most of all the best of friends.

Supplementary materials

Supplementary material associated with this article can be found, in the online version, at doi:10.1016/j.mcat.2022.112476.

References

[1] P. Nejat, F. Jomehzadeh, M.M. Taheri, M. Gohari, M.Z.A. Majid, A global review of energy consumption, CO_2 emissions and policy in the residential sector (with an overview of the top ten CO_2 emitting countries), Renew. Sustain. Energy Rev. 43 (2015) 843–862.
[2] J.G.J. Olivier, J.A.H.W. Peters, Trends in global CO2 and total greenhouse gas emissions 2019 Report.
[3] CO2.earth Are we Stabilizing Yet? Prooxygen Web Site https://www.co2.earth/(accessed 20th September 2021).
[4] P. Poizot, F. Dolhem, Clean energy new deal for a sustainable world: from non-CO_2 generating energy sources to greener electrochemical storage devices, Energy Environ. Sci. 4 (2011) 2003–2019.
[5] L. Schlapbach, A. Züttel, Hydrogen-storage materials for mobile applications, Nature 414 (2001) 353–358.
[6] T. He, P. Pachfule, H. Wu, Q. Xu, P. Chen, Hydrogen carriers, Nat. Rev. Mater. 1 (2016) 16059.
[7] M. Hirscher, V.A. Yartys, M. BariccoJose, B. von Colbe, D. Blanchard, R. C. Bowman, D.P. Broom, C.E. Buckley, F. Chang, P. Chen, Y.W. Cho, J.C. Crivello, F. Cuevas, W.I.F. David, P.E. de Jongh, R.V. Denys, M. Dornheim, M. Felderhoff, Y. Filinchuk, G.E. Froudakis, D.M. Grant, et al., Materials for hydrogen-based energy storage – past, recent progress and future outlook, J. Alloy. Compd. 827 (2020), 153548.
[8] R. Abbasi, B.P. Setzler, S. Lin, J. Wang, Y. Zhao, H. Xu, B. Pivovar, B. Tian, X. Chen, G. Wu, Y. Yan, A Roadmap to low-cost hydrogen with hydroxide exchange membrane electrolyzers, Adv. Mater. 31 (2019), 1805876.
[9] I. Vincent, D. Bessarabov, Low-cost hydrogen production by anion exchange membrane electrolysis: a review, Renew. Sustain. Energy Rev. 81 (2018) 1690–1704.
[10] J.P. Hughes, J. Clipsham, H. Chavushoglu, S.J. Rowley-Neale, C.E. Banks, Polymer electrolyte electrolysis: a review of the activity and stability of non-precious metal hydrogen evolution reaction and oxygen evolution reaction catalysts, Renew. Sustain. Energy Rev. 139 (2021), 110709.
[11] X. Zou, Y. Zhang, Noble metal-free hydrogen evolution catalysts for water splitting, Chem. Soc. Rev. 44 (2015) 5148–5180.
[12] C. Li, J.B. Bae, The promise of hydrogen production from alkaline anion exchange membrane electrolyzers, Nano Energy 87 (2021), 106162.

[13] U. Eberle, M. Felderhoff, F. Schüth, Chemical and physical solutions for hydrogen storage, Angew. Chem. Int. Ed. 48 (2009) 6608–6630.

[14] Q. Sun, N. Wang, Q. Xu, J. Yu, Nanopore-supported metal nanocatalysts for efficient hydrogen generation from liquid-phase chemical hydrogen storage materials, Adv. Mater. 32 (2020), 2001818.

[15] C. Lang, Y. Jia, X. Yao, Recent advances in liquid-phase chemical hydrogen storage, Energy Storage Mater. 26 (2020) 290–312.

[16] L. Lu, H. Zhang, S. Zhang, F. Li, A family of high-efficiency hydrogen-generation catalysts based on ammonium species, Angew. Chem. Int. Ed. 54 (2015) 9328–9332.

[17] B. Zhu, R. Zou, Q. Xu, Metal–organic framework-based catalysts for hydrogen evolution, Adv. Energy Mater. 8 (2018), 1801193.

[18] S. Akbayraka, S. Özkar, Ammonia borane as hydrogen storage materials, Int. J. Hydrog. Energy 43 (2018) 18592–18606.

[19] C. Yüksel, A. Senem, K. Gülbay, C.O. Colpan, A review on the catalysts used for hydrogen production from ammonia borane, Int. J. Hydrog. Energy 45 (2020) 3414–3434.

[20] A. Staubitz, A.P.M. Robertson, I. Manners, Ammonia-borane and related compounds as dihydrogen sources, Chem. Rev. 110 (2010) 4079–4124.

[21] N.Z.A.K. Khafid, Z. Yaakob, K.L. Lim, S.N. Timmiati, The kinetics of lightweight solid-state hydrogen storage materials: a review, Int. J. Hydrog. Energy 41 (2016) 13131–13151.

[22] M. Yadav, Q. Xu, Liquid-phase chemical hydrogen storage materials, Energy Environ. Sci. 5 (2012) 9698–9725.

[23] U.B. Demirci, P. Miele, Sodium borohydride versus ammonia borane, in hydrogen storage and direct fuel cell applications, Energy Environ. Sci. 2 (2009) 627–637.

[24] X. Liu, X. Zhang, D.S. Li, S. Zhang, Q. Zhang, Recent advances in the "on–off" approaches for on-demand liquid-phase hydrogen evolution, J. Mater. Chem. A 9 (2021) 18164–18174.

[25] A.F. Dalebrook, W. Gan, M. Grasemann, S. Moret, G. Laurenczy, Hydrogen storage: beyond conventional methods, Chem. Commun. 49 (2013) 8735–8751.

[26] E.Y. Marrero-Alfonso, A.M. Beaird, T.A. Davis, M.A. Matthews, Hydrogen generation from chemical hydrides, Ind. Eng. Chem. Res. 48 (2009) 3703–3712.

[27] H.N. Abdelhamid, A review on hydrogen generation from the hydrolysis of sodium borohydride, Int. J. Hydrog. Energy 46 (2021) 726–765.

[28] D.M.F. Santos, C.A.C. Sequeira, Sodium borohydride as a fuel for the future, Renew. Sustain. Energy Rev. 15 (2011) 3980–4001.

[29] S.S. Muira, X. Yao, Progress in sodium borohydride as a hydrogen storage material: development of hydrolysis catalysts and reaction systems, Int. J. Hydrog. Energy 36 (2011) 5983–5997.

[30] N. Patel, A. Miotello, Progress in Co–B related catalyst for hydrogen production by hydrolysis of boron-hydrides: a review and the perspectives to substitute noble metals, Int. J. Hydrog. Energy 40 (2015) 1429–1464.

[31] B.H. Liu, Z.P. Li, A review: hydrogen generation from borohydride hydrolysis reaction, J. Power Sources 187 (2009) 527–534.

[32] U.B. Demirci, Impact of H.I. Schlesinger's discoveries upon the course of modern chemistry on B–(N–)H hydrogen carriers, Int. J. Hydrog. Energy 42 (2017) 21048–21062.

[33] P. Brack, S.E. Dann, K.G.U Wijayantha, Heterogeneous and homogenous catalysts for hydrogen generation by hydrolysis of aqueous sodium borohydride ($NaBH_4$) solutions, Energy Sci. Eng. 3 (2015) 174–188.

[34] K. Sordakis, C. Tang, L.K. Vogt, H. Junge, P.J. Dyson, M. Beller, G. Laurenczy, Homogeneous catalysis for sustainable hydrogen storage in formic acid and alcohols, Chem. Rev. 118 (2017) 372–433.

[35] N. Onishi, G. Laurenczy, M. Beller, Y. Himeda, Recent progress for reversible homogeneous catalytic hydrogen storage in formic acid and in methanol, Coord. Chem. Rev. 373 (2018) 317–332.

[36] C.W. Hamilton, R.T. Baker, A. Staubitz, I. Manners, B–N compounds for chemical hydrogen storage, Chem. Soc. Rev. 38 (2009) 279–293.

[37] N. Onishi, M. Iguchi, X. Yang, R. Kanega, H. Kawanami, Q. Xu, Y. Himeda, Development of effective catalysts for hydrogen storage technology using formic acid, Adv. Energy Mater. 9 (2019), 1801275.

[38] T. Shimbayashi, K. Fujita, Metal-catalyzed hydrogenation, and dehydrogenation reactions for efficient hydrogen storage, Tetrahedron 76 (2020), 130946.

[39] L. Luconi, G. Tuci, G. Giambastiani, A. Rossin, M. Peruzzini, H_2 production from lightweight inorganic hydrides catalyzed by 3d transition metals, Int. J. Hydrog. Storage 44 (2019) 25746–25776.

[40] Z. Li, Q. Xu, Metal-nanoparticle-catalyzed hydrogen generation from formic, Acc. Chem. Res. 50 (2017) 1449–1458.

[41] W.W. Zhan, Q.L. Zhu, Q. Xu, Dehydrogenation of ammonia borane by metal nanoparticle catalysts, ACS Catal. 6 (2016) 6892–6905.

[42] C. Wang, D. Astruc, Recent developments of nanocatalyzed liquid-phase hydrogen generation, Chem. Soc. Rev. 50 (2021) 3437–3484.

[43] C. Wang, Q. Wang, F. Fu, D. Astruc, Hydrogen generation upon nanocatalyzed hydrolysis of hydrogen-rich boron derivatives: recent developments, Acc. Chem. Res. 53 (2020) 2483–2493.

[44] X.F. Yang, A. Wang, B. Qiao, J. Li, J. Liu, T. Zhang, Single-atom catalysts: a new frontier in heterogeneous catalysis, Acc. Chem. Res. 46 (2013) 1740–1748.

[45] G. Schmid, Nanoparticles: From Theory to Applications, Wiley-VCH, Weinheim, 2004, pp. 1–359.

[46] A.M. Huang, A. Su, Y.C. Liu, Hydrogen generator system using Ru catalyst for PEMFC (proton exchange membrane fuel cell) applications, Energy 51 (2013) 230–236.

[47] J. Kim, T. Kim, Compact PEM fuel cell system combined with all-in-one hydrogen generator using chemical hydride as a hydrogen source, Appl. Energy 160 (2015) 945–953.

[48] K. Kim K, T. Kim T, K. Lee K, S. Kwon, Fuel cell system with sodium borohydride as hydrogen source for unmanned aerial vehicles, J. Power Sources 196 (2011) 9069–9075.

[49] X. Qu, R. Jiang, Q. Li, F. Zeng, X. Zheng, Z. Xu, C. Chen, J. Peng, The hydrolysis of ammonia borane catalyzed by NiCoP/OPC-300 nanocatalysts: high selectivity and efficiency, and mechanism, Green Chem. 21 (2019) 850–860.

[50] Y.Y. Cai, X.H. Li, Y.N. Zhang, X. Wei, K.X. Wang, J.S. Chen, Highly efficient dehydrogenation of formic acid over a palladium-nanoparticle-based Mott–Schottky photocatalyst, Angew. Chem. Int. Ed. 52 (2013) 11822–11825.

[51] F.Z. Song, Q.L. Zhu, X. Yang, W.W. Zhan, P. Pachfule, N. Tsumori, Q. Xu, Metal–organic framework templated porous carbon-metal oxide/reduced graphene oxide as superior support of bimetallic nanoparticles for efficient hydrogen generation from formic acid, Adv. Energy Mater. 8 (2018), 1701416.

[52] B. Zhu, R. Zou, Q. Xu, Metal–organic framework-based catalysts for hydrogen evolution, Adv. Energy Mater. 8 (2018), 1801193.

[53] P.Z. Li, A. Aijaz, Q. Xu, Highly dispersed surfactant-free nickel nanoparticles and their remarkable catalytic activity in the hydrolysis of ammonia borane for hydrogen generation, Angew. Chem. Int. Ed. 51 (2012) 6753–6756.

[54] W. Chen, D. Li, C. Peng, G. Qian, X. Duan, D. Chen, X. Zhou, Mechanistic and kinetic insights into the Pt-Ru synergy during hydrogen generation from ammonia borane over PtRu/CNT nanocatalysts, J. Catal. 356 (2017) 186–196.

[55] Y.T. Li, X.L. Zhang, Z.K. Peng, P. Liu, X.C. Zheng, Hierarchical porous g-C_3N_4 coupled ultrafine RuNi alloys as extremely active catalysts for the hydrolytic dehydrogenation of ammonia borane, ACS Sustain. Chem. Eng. 8 (2020) 8458–8468.

[56] X. Li, C. Zhang, M. Luo, Q. Yao, Z.H. Lu, Ultrafine Rh nanoparticles confined by nitrogen-rich covalent organic frameworks for methanolysis of ammonia borane, Inorg. Chem. Front. 7 (2020) 1298–1306.

[57] R. Ding, Q. Chen, Q. Luo, L. Zhou, Y. Wang, Y. Zhang, G. Fan, Salt template-assisted in situ construction of Ru nanoclusters and porous carbon: excellent catalysts toward hydrogen evolution, ammonia-borane hydrolysis, and 4-nitrophenol reduction, Green Chem. 22 (2020) 835–842.

[58] M. Zahmakiran, T. Ayvali, S. Akbayrak, S. Caliskan, D. Celik, S. Özkar, Zeolite framework stabilized nickel(0) nanoparticles: active and long-lived catalyst for hydrogen generation from the hydrolysis of ammonia-borane and sodium borohydride, Catal. Today 170 (2011) 76–84.

[59] S. Akbayrak, Z. Özçifçi, A.J. Tabak, Noble metal nanoparticles supported on activated carbon: highly recyclable catalysts in hydrogen generation from the hydrolysis of ammonia borane, J. Colloid Sci. 546 (2019) 324–332.

[60] L. Yin, T. Zhang, K. Dai, B. Zhang, X. Xiang, H. Shang, Ultrafine PtCo alloy nanoclusters confined in N-doped mesoporous carbon spheres for efficient ammonia borane Hydrolysis, ACS Sustain. Chem. Eng. 9 (2021) 822–832.

[61] Q. Sun, N. Wang, Q. Bing, R. Si, J. Liu, R. Bai, P. Zhang, M. Jia, J. Yu, Subnanometric hybrid Pd-M$(OH)_2$, M = Ni, Co, clusters in zeolites as highly efficient nanocatalysts for hydrogen generation, Chem. 3 (2017) 477–493.

[62] N. Wang, Q. Sun, R. Bai, X. Li, G. Guo, J. Yu, In situ confinement of ultrasmall Pd clusters within nanosized silicalite-1 zeolite for highly efficient catalysis of hydrogen generation, J. Am. Chem. Soc. 138 (2016) 7484–7487.

[63] Q. Sun, N. Wang, T. Zhang, R. Bai, A. Mayoral, P. Zhang, Q. Zhang, O. Terasaki, J. Yu, Zeolite-encaged single-atom rhodium catalysts: highly efficient hydrogen generation and shape-selective tandem hydrogenation of nitroarenes, Angew. Chem. Int. Ed. 58 (2019) 18570–18576.

[64] M. Zahmakiran, S. Özkar, Zeolite-Confined Ruthenium(0) nanoclusters catalyst: record catalytic activity, reusability, and lifetime in hydrogen generation from the hydrolysis of sodium borohydride, Langmuir 25 (2009) 2667–2678.

[65] Q. Sun, N. Wang, R. Bai, Y. Hui, T. Zhang, D.A. Do, P. Zhang, L. Song, S. Miao, J. Yu, Synergetic effect of ultrasmall metal clusters and zeolites promoting hydrogen generation, Adv. Sci. 6 (2019), 1802350.

[66] P. Verma, K. Yuan, Y. Kuwahara, K. Moria, H. Yamashita, Enhancement of plasmonic activity by Pt/Ag bimetallic nanocatalyst supported on mesoporous silica in the hydrogen production from hydrogen storage material, Appl. Catal. B 223 (2018) 10–15.

[67] N. Patel, R. Fernandes, S. Gupta, R. Edla, D.C. Kothari, A. Miotello, Co-B catalyst supported over mesoporous silica for hydrogen production by catalytic hydrolysis of ammonia borane: a study on influence of pore structure, Appl. Catal. B 140-141 (2013) 125–132.

[68] K. Mori, Y. Futamura, S. Masuda, H. Kobayashi, H. Yamashita, Controlled release of hydrogen isotope compounds and tunnelling effect in the heterogeneously catalyzed formic acid dehydrogenation, Nat. Commun. 10 (2019) 4094.

[69] H. Zhong, Y. Su, C. Cui, F. Zhou, X. Li, R. Wang, Palladium Nanoparticles supported by carboxylate-functionalized porous organic polymers for additive-free hydrogen generation from formic acid, ACS Sustain. Chem. Eng. 5 (2017) 8061–8069.

[70] C. Cui, Y. Tang, M.A. Ziaee, D. Tian, R. Wang, Highly Dispersed Ultrafine Palladium nanoparticles enabled by functionalized porous organic polymer for additive-free dehydrogenation of formic acid, ChemCatChem 10 (2018) 1431–1437.

[71] Q.L. Zhu, J. Li, Q. Xu, Immobilizing metal nanoparticles to metal–organic frameworks with aize and location control for optimizing catalytic performance, J. Am. Chem. Soc. 135 (2013) 10210–10213.

[72] C. Wang, J. Tuninetti, Z. Wang, C. Zhang, R. Ciganda, L. Salmon, S. Moya, J. Ruiz, D. Astruc, Hydrolysis of ammonia-borane over Ni/ZIF-8 nanocatalyst: high efficiency, mechanism, and controlled hydrogen release, J. Am. Chem. Soc. 139 (2017) 11610–11615.

[73] F. Fu, C. Wang, Q. Wang, A.M. Martinez-Villacorta, A. Escobar, H. Chong, X. Wang, S. Moya, E. Salmon, E. Fouquet, J. Ruiz, D. Astruc, Highly selective and

sharp volcano-type synergistic Ni_2Pt@ZIF-8-catalyzed hydrogen evolution from ammonia borane hydrolysis, J. Am. Chem. Soc. 140 (2018) 10034–10042.
[74] X. Gu, Z.H. Lu, H.L. Jiang, T. Akita, Q. Xu, Synergistic catalysis of metal–organic framework-immobilized Au–Pd nanoparticles in dehydrogenation of formic acid for chemical hydrogen storage, J. Am. Chem. Soc. 133 (2011) 11822–11825.
[75] C. Luo, F. Fu, X. Yang, J. Wei, C. Wang, J. Zhu, D. Huang, D. Astruc, P. Zhao, Highly efficient and selective Co@ZIF-8 nanocatalyst for hydrogen release from sodium borohydride hydrolysis, ChemCatChem 11 (2019) 1643–1644.
[76] S. Zhang, L. Zhou, M. Chen, Amine-functionalized MIL-53(Al) with embedded ruthenium nanoparticles as a highly efficient catalyst for the hydrolytic dehydrogenation of ammonia borane, RSC Adv. 8 (2018) 12282–12291.
[77] DD Tuan, KYA. Lin, Ruthenium-supported on ZIF-67 as an enhanced catalyst for hydrogen generation from hydrolysis of sodium borohydride, Chem. Eng. J. 351 (2018) 48–55.
[78] N. Kang, R. Djeda, Q. Wang, F. Fu, J. Ruiz, J.L. Pozzo, D. Astruc, Efficient “Click”-Dendrimer-supported synergistic bimetallic nanocatalysis for hydrogen evolution by sodium borohydride hydrolysis, ChemCatChem 11 (2019) 2341–2349.
[79] Q. Wang, F. Fu, A. Escobar, S. Moya, J. Ruiz, D. Astruc, Click” Dendrimer-stabilized nanocatalysts for efficient hydrogen release upon ammonia-borane hydrolysis, ChemCatChem 10 (2018) 2673–2680.
[80] Q. Wang, F Fu, S. Yang, M. Martinez Moro, M. de los Angeles Ramirez, S. Moya, L. Salmon, J. Ruiz, D. Astruc, Dramatic synergy in CoPt nanocatalysts stabilized by “click” dendrimers for evolution of hydrogen from hydrolysis of ammonia borane, ACS Catal. 9 (2019) 1110–1119.
[81] G. Lu, S. Li, Z. Guo, O.K. Farha, B.G. Hauser, X. Qi, Y. Wang, X. Wang, S. Han, X. Li, J.S. DuChene, H. Zhang, Q. Zhang, X. Chen, J. Ma, S.C.J. Loo, W.D. Wei, Y. Yang, J.T. Hupp, F. Huo, Imparting functionality to a metal–organic framework material by controlled nanoparticle encapsulation, Nat. Chem. 4 (2012) 310–316.
[82] K.M. Choi, K. Na, G.A. Somorjai, O.M. Yaghi, Chemical environment control and enhanced catalytic performance of platinum nanoparticles embedded in nanocrystalline metal–organic frameworks, J. Am. Chem. Soc. 137 (2015) 7810–7815.
[83] K. Na, K.M. Choi, O.M. Yaghi, G.A. Somorjai, Metal Nanocrystals embedded in single nanocrystals of MOFs give unusual selectivity as heterogeneous catalysts, Nano Lett. 14 (2014) 5979–5983.
[84] B. Rungtaweevoranit, B. Baek, J.R. Araujo, B.S. Archanjo, K.M. Choi, O.M. Yaghi, G.A Somorjai, Copper nanocrystals encapsulated in Zr-based metal–organic frameworks for highly selective CO_2 hydrogenation to methanol, Nano Lett. 16 (2016) 7645–7649.
[85] A. Aijaz, A. Karkamkar, A.Y.J. Choi, N. Tsumori, E. Rönnebro, T. Autrey, H. Shioyam, Q. Xu, Immobilizing highly catalytically active Pt nanoparticles inside the pores of metal–organic framework: a double solvents approach, J. Am. Chem. Soc. 134 (2012) 13926–13929.
[86] M. Zha, K. Yuan, Y. Wang, G. Li, J. Guo, G.L. Gu, W. Hu, H. Zhao, Z. Tang, Metal–organic frameworks as selectivity regulators for hydrogenation reactions, Nature 539 (2016) 76–80.
[87] K.M. Choi, D. Kim, B. Rungtaweevoranit, C.A. Trickett, J.T.D. Barmanbek, A. SS. Alshammari, P. Yang, O.M. Yaghi, Plasmon-enhanced photocatalytic CO_2 conversion within metal–organic frameworks under visible light, J. Am. Chem. Soc. 139 (2017) 356–362.
[88] Q. Yang, Q. Xu, H.L. Jiang, Metal–organic frameworks meet metal nanoparticles: synergistic effect for enhanced catalysis, Chem. Soc. Rev. 46 (2017) 4774–474808.
[89] D. Astruc, F. Lu, J.R. Aranzaes, Nanoparticles as recyclable catalysts: the frontier between homogeneous and heterogeneous catalysis, Angew. Chem. Int. Ed. 44 (2005) 7852–7872.
[90] E. Gross, J.P.C. Liu, D.F. Toste, G.A. Somorjai, Control of selectivity in heterogeneous catalysis by tuning nanoparticle properties and reactor residence time, Nat. Chem. 4 (2012) 947–952.
[91] M. Sankar, N. Dimitratos, P.J. Miedziak, P.P. Wells, J.J. Kiely, G.J. Hutchings, Designing bimetallic catalysts for a green and sustainable future, Chem. Soc. Rev. 41 (2012) 8099–8139.
[92] M. Sankar, Q. He, R.V. Engel, M.A. Sainna, A.J. Logsdail, A. Rolda, D.J. Willock, N. Agarwal, C.J. Kiely, G.J. Hutchings, Role of the support in gold-containing nanoparticles as heterogeneous catalysts, Chem. Rev. 120 (2020) 3890–3938.
[93] M.B. Gawande, A. Goswami, F.X. Felpin, T. Asefa, X. Huang, R. Silva, X. Zou, R. Zboril, R.S. Varma, Cu and Cu-based nanoparticles: synthesis and applications in catalysis, Chem. Rev. 116 (2016) 3722–3811.
[94] K. Loza, M. Heggen, M. Epple, Synthesis, structure, properties, and applications of bimetallic nanoparticles of noble metals, Adv. Funct. Mater. 30 (2020), 1909260.
[95] S.M.H. Chopani, S. Asadi, M.M. Heravi, Application of bimetallic and trimetallic nanoparticles supported on graphene as novel heterogeneous catalysts in the reduction of nitroarenes, homo-coupling, Suzuki-Miyaura and Sonogashira reactions, Curr. Org. Chem. 24 (2020) 2216–2234.
[96] S. Anand, D. Pinheiro, K.R.S. Devi, Recent advances in hydrogenation reactions using bimetallic nanocatalysts: a review, Asian J. Org. Chem. 10 (2021) 3068–3100.
[97] E. Kuna, D. Mrdenovic, M. Jönsson-Niedziółka, P. Pieta, I.S. Pieta, Bimetallic nanocatalysts supported on graphitic carbon nitride for sustainable energy development: the shape-structure–activity relation, Nanoscale Adv. 3 (2021) 1342–1351.
[98] J.D. Scholten, B.C. Leal, J. Dupont, Transition metal nanoparticle catalysis in ionic liquids, ACS Catal. 2 (2012) 184–200.
[99] S. Doherty, Catalysis in ionic liquids: from catalysis synthesis to applications, in: C. Hardacre, V. Parvulescu (Eds.), RSC Catalysis Series, The Royal Society of Chemistry, 2014, pp. 44–308.
[100] P. Migowski, K.L. Luska, W. Leitner, in Nanocatalysts in ionic liquids; M. H. G. Prechtl, Ed.: Wiley VCH: Weinheim, 2016.
[101] C. Janiak, Ionic liquids for the synthesis and stabilization of metal nanoparticles, Z. Naturforsch. 68b (2013) 1059–1089.
[102] A.S. Pensando, A.A.H. Pádua, Solvation and stabilization of metallic nanoparticles in ionic liquids, Angew. Chem. Int. Ed. 50 (2011) 8683–8687.
[103] A. Kraynov, T.E. Müller, Concepts for the Stabilization of Metal Nanoparticles in Ionic Liquids, Applications of Ionic Liquids in Science and Technology, Scott Handy, IntechOpen, 2011, https://doi.org/10.5772/22111.
[104] K.L. Luska, A. Moores, Functionalized ionic liquids for the synthesis of metal nanoparticles and their application in catalysis, ChemCatChem 4 (2012) 1534–1546.
[105] B.C. Leal, C.S. Consorti, G. Machado, J. Dupont, Palladium metal nanoparticles stabilized by ionophilic ligands in ionic liquids: synthesis and application in hydrogenation reaction, Catal. Sci. Technol. 5 (2015) 903–909.
[106] Z. Wu, H. Jiang, Efficient palladium and ruthenium nanocatalysts stabilized by phosphine functionalized ionic liquid for selective hydrogenation, RSC Adv. 5 (2015) 34622–34629.
[107] Y. Hu, Y. Yu, Z. Hou, H. Li, X. Zhao, B. Feng, Biphasic hydrogenation of olefins by functionalized ionic liquid-stabilized palladium nanoparticles, Adv. Synth. Catal. 350 (2008) 2077–2085.
[108] K.L. Luska, A. Moores, Improved stability and catalytic activity of palladium nanoparticle catalysts using phosphine-functionalized imidazolium ionic liquids, Adv. Synth. Catal. 353 (2011) 3167–3177.
[109] S.A. Stratton, K.L. Luska, A. Moores, Rhodium nanoparticles stabilized with phosphine functionalized imidazolium ionic liquids as recyclable arene hydrogenation catalysts, Catal. Today 183 (2012) 96–100.
[110] H.Y. Jiang, X.X. Zheng, Tuning the chemoselective hydrogenation of aromatic ketones, aromatic aldehydes and quinolines catalyzed by phosphine functionalized ionic liquid stabilized ruthenium nanoparticles, Catal. Sci. Technol. 5 (2015) 3728–3734.
[111] H.Y. Jiang, X.X. Zheng, Phosphine-functionalized ionic liquid-stabilized rhodium nanoparticles for selective hydrogenation of aromatic compounds, Appl. Catal. A 499 (2015) 118–123.
[112] For a recent insightful review describing the use of covalently supported ionic liquids in catalysis see: F. Giacalone, M. Gruttadauria, Covalently supported ionic liquid phases: an advanced class of recyclable catalytic systems, ChemCatChem 8 (2016) 664–684.
[113] For a relevant and informative account of metal nanoparticles immobilised on molecularly modified surfaces see: A. Bordet, W. Leitner, Metal nanoparticles immobilized on molecularly modified surfaces: versatile catalytic systems for controlled hydrogenation and hydrogenolysis, Acc. Chem. Res. 54 (2021) 2144–2157.
[114] W. Qian, J. Texter, F. Yam, Frontiers in poly(ionic liquid)s: syntheses and applications, Chem. Soc. Rev. 46 (2017) 1124–1159.
[115] H. Li, P.S. Bhadury, B. Song, S. Yang, Immobilized functional ionic liquids: efficient, green, and reusable catalysts, RSC Adv. 2 (2012) 12525–12551.
[116] K. Manojkumar, A. Sivaramakrishna, K. Vijayakrishna, A short review on stable metal nanoparticles using ionic liquids, supported ionic liquids, and poly(ionic liquids), J. Nanopart. Res. 18 (2016) 103.
[117] S. Montolio, C. Vicent, V. Aseyev, I. Alfonso, M.I. Burguete, H. Tenhu, E. García-Verdugo, S.V. Luis, AuNP–polymeric ionic liquid composite multicatalytic nanoreactors for one-pot cascade reactions, ACS Catal. 6 (2016) 7230–7237.
[118] L. Lu, S. Zou, B. Fang, The critical impacts of ligands on heterogeneous nanocatalysis: a review, ACS Catal. 11 (2021) 6020–6058.
[119] S. Doherty, J.G. Knight, T. Backhouse, E. Abood, H. Alshaikh, I.A.J. Fairlamb, R. A. Bourne, T.W. Chamberlain, R. Stones, Highly efficient aqueous phase chemoselective hydrogenation of α,β-unsaturated aldehydes catalysed by phosphine-decorated polymer immobilized IL-stabilized PdNPs, Green Chem. 19 (2017) 1635–1641.
[120] S. Doherty, J.G. Knight, T. Backhouse, A. Bradford, F. Saunders, R.A. Bourne, T. W. Chamberlain, R. Stones, A. Clayton, K.J.R. Lovelock, Highly efficient aqueous phase reduction of nitroarenes catalyzed by phosphine-decorated polymer immobilized ionic liquid stabilized PdNPs, Catal. Sci. Technol. 8 (2018) 1454–1467.
[121] S. Doherty, J.G. Knight, T. Backhouse, E. Abood, H. Alshaikh, A. Clemmet, J. R. Ellison, R.A. Bourne, T.W. Chamberlain, R. Stones, I.A.J. Fairlamb, K.J. R. Lovelock, heteroatom donor-decorated polymer-immobilized ionic liquid stabilized palladium nanoparticles: efficient catalysts for room-temperature Suzuki-Miyaura cross-coupling in aqueous media, Adv. Synth. Catal. 360 (2018) 3716–3731.
[122] S. Doherty, J.G. Knight, T. Backhouse, W. Simpson, W. Paget, E. Abood, R. A. Bourne, T.W. Chamberlain, R. Stones, K.J.R. Lovelock, J.M. Seymour, M. A. Isaacs, H. Daley, C. Hardacre, N.H. Rees, Highly selective and solvent-dependent reduction of nitrobenzene to N-phenylhydroxylamine, azoxybenzene, and aniline catalyzed by phosphine-modified polymer immobilized ionic liquid-stabilized AuNPs, ACS Catal. 9 (2019) 4777–4791.
[123] S. Doherty, J.G. Knight, T. Backhouse, T.S.T. Tran, F. Stahl, H.Y. Alharbi, T. W. Chamberlain, R.A. Bourne, R. Stones, J.P. White, Z. Aslam, C. Hardacre, H. Daly, J. Hart, R.H. Temperton, J.N. O'Shea, N.H Rees, Highly efficient and selective aqueous phase hydrogenation of aryl ketones, aldehydes, furfural and levulinic acid and its ethyl ester catalyzed by phosphine oxide-decorated polymer immobilized ionic liquid stabilized ruthenium nanoparticles, Catal. Sci. Technol. 12 (2022) 3549–3567.
[124] Y. Gong, H. Zhong, W. Lu, B. Zhang, S. Hu, R. Wang, General synthetic route toward highly dispersed ultrafine Pd–Au alloy nanoparticles enabled by

imidazolium-based organic polymers, ACS Appl. Mater. Interfaces 10 (2018) 776–786.

[125] S. Doherty, J.G. Knight, H.Y. Alharbi, R. Paterson, C. Wills, C. Dixon, L. Šiller, T. W. Chamberlain, A. Griffiths, S.M. Collins, K-J. Wu, M.D. Simmons, R.A. Bourne, K.R.J. Lovelock, J. Seymour, Efficient hydrolytic hydrogen evolution from sodium norohydride catalyzed by polymer immobilized ionic liquid-stabilized platinum nanoparticles, ChemCatChem (2022), https://doi.org/10.1002/cctc.202101752R1.

[126] G. Chen, C. Xu, X. Huang, J. Ye, L. Gu, G. Li, Z. Tang, B. Wu, H. Yang, Z. Zhao, Z. Zhou, G. Fu, N. Zheng, Interfacial electronic effects control the reaction selectivity of platinum catalysts, Nat. Mater. 15 (2016) 564–569.

[127] E.H. Boymans, P.T. Witte, D. Vogt, A study on the selective hydrogenation of nitroaromatics to N-arylhydroxylamines using a supported Pt nanoparticle catalyst, Catal. Sci. Technol. 5 (2015) 176–183.

[128] J. Tan, J. Cui, G. Ding, T. Deng, Y. Zhu, Y.W. Li, Efficient aqueous hydrogenation of levulinic acid to γ-valerolactone over a highly active and stable ruthenium catalyst, Catal. Sci. Technol. 6 (2016) 1469–1475.

[129] J. Mondal, S.K. Kundu, W.K.H. Ng, R. Singuru, P. Borah, H. Hirao, Y. Zhao, A. Bhaumik, Fabrication of ruthenium nanoparticles in porous organic polymers: towards advanced heterogeneous catalytic nanoreactors, Chem. Eur. J. 21 (2015) 19016–19027.

[130] M. Guo, C. Li, Q. Yang, Accelerated catalytic activity of Pd NPs supported on amine-rich silica hollow nanospheres for quinoline hydrogenation, Catal. Sci. Technol. 7 (2017) 2221–2227.

[131] S.G. Kwon, G. Krylova, A. Sumer, M.M. Schwart, E.M. Bunel, C.L. Marshall, S. Chattopadhyay, B. Le, J. Jellinek, E.V. Shevchenko, Capping ligands as selectivity switchers in hydrogenation reactions, Nano Lett. 12 (2012) 5382–5388.

[132] W. Long, N.A. Brunelli, S.A. Didas, E.W. Ping, C.W. Jones, Aminopolymer–silica composite-supported Pd catalysts for selective hydrogenation of alkynes, ACS Catal. 3 (2013) 1700–1708.

[133] F.P. da Silva, J.L. Fiorio, L.M. Rossi, Tuning the catalytic activity and selectivity of Pd nanoparticles using ligand-modified supports and surfaces, ACS Omega 2 (2017) 6014–6022.

[134] Z. Guo, C. Xiao, R.V. Maligal-Ganesh, L. Zhou, T.W. Goh, X. Li, D. Tesfagaber, A. Thiel, W. Huang, Pt Nanoclusters confined within metal–organic framework cavities for chemoselective cinnamaldehyde hydrogenation, ACS Catal. 4 (2014) 1340–1348.

[135] Y. Wei, Y. Wang, L. Wei, X. Zhao, X. Zhou, H. Liu, Highly efficient and reactivated electrocatalyst of ruthenium electrodeposited on nickel foam for hydrogen evolution from NaBH4 alkaline solution, Int. J. Hydrog. Energy 43 (2018) 592–600.

[136] R. Fiorenza, S. Scirè, A.M. Venezia, Carbon supported bimetallic Ru-Co catalysts for H_2 production through $NaBH_4$ and NH_3BH_3 hydrolysis, Int. J. Energy Res. 42 (2018) 1183–1195.

[137] L. Semiz, N. Abdullayeva, M. Sankir, Nanoporous Pt and Ru catalysts by chemical dealloying of Pt-Al and Ru-Al alloys for ultrafast hydrogen generation, J. Alloy. Compd. 744 (2018) 110–115.

[138] S.C. Amendola, S.L. Sharp-Goldman, M.S. Janjua, N.C. Spencer, M.T. Kelly, P. J. Petillo, M.A. Binder, Safe, portable, hydrogen gas generator using aqueous borohydride solution and Ru catalyst, Int. J. Hydrog. Energy 25 (2000) 969–975.

[139] Y. Liang, H.B. Dai, L.P. Ma, P. Wang, H.M. Cheng, Hydrogen generation from sodium borohydride solution using a ruthenium supported on graphite catalyst, Int. J. Hydrog. Energy 35 (2010) 3023–3028.

[140] Z. Liu, B. Guo, S.H. Chan, E.H. Tang, L. Hong, Pt and Ru dispersed on $LiCoO_2$ for hydrogen generation from sodium borohydride solution, J. Power Sources 76 (2008) 306–311.

[141] Y. Li, Q. Zhang, N. Zhang, L. Zhu, J. Zheng, B.H. Chen, Ru-RuO_2/C as an efficient catalyst for the sodium borohydride hydrolysis to hydrogen, Int. J. Hydrog. Energy 38 (2013) 13360–13367.

[142] Y. Shang, R. Chen, Semiempirical hydrogen generation model using concentrated sodium borohydride solution, Energy Fuels 20 (2006) 2149–2154.

[143] J.C. Ingersoll, N. Mani, J.C. Thenmozhiyal, A. Muthaiah, Catalytic hydrolysis of sodium borohydride by a novel nickel-cobalt-boride catalyst, J. Power Sources 173 (2007) 450–457.

[144] W. Ye, H. Zhang, D. Xu, L. Ma, B. Yi, Hydrogen generation utilizing alkaline sodium borohydride solution and supported cobalt catalyst, J. Power Sources 164 (2007) 544–548.

[145] N. Patel, R. Fernandes, A. Miotello, Hydrogen generation by hydrolysis of $NaBH_4$ with efficient Co-P-B catalyst: a kinetic study, J. Power Sources 188 (2009) 411–420.

[146] D. Hua, Y. Hanxi, A. Xinping, C. Chuansin, Hydrogen production from catalytic hydrolysis of sodium borohydride solution using nickel boride catalyst, Int. J. Hydrog. Energy 28 (2003) 1095–1100.

[147] Q. Zhang, Y. Wu, X. Sun, J. Ortega, Kinetics of catalytic hydrolysis of stabilized sodium borohydride solutions, Ind. Eng. Chem. Res. 46 (2007) 1120.

[148] J. Lee, K.Y. Kong, C.R. Jung, E. Cho, S.P. Yoon, J. Hana, T.G. Lee, S.W. Nam, A structured Co–B catalyst for hydrogen extraction from $NaBH_4$ solution, Catal. Today 120 (2007) 305–310.

[149] M. Zahmakiran, S. Özkar, Water dispersible acetate stabilized ruthenium(0) nanoclusters as catalyst for hydrogen generation from the hydrolysis of sodium borohyride, J. Mol. Catal. A Chem. 258 (2006) 95–103.

[150] S.C. Amendola, S.L. Sharp-Goldman, M.S. Janjua, M.T. Kelly, P.J. Petillo, M. A. Binder, An ultrasafe hydrogen generator: aqueous, alkaline borohydride solutions and Ru catalyst, J. Power Sources 186 (2000) 186–189.

[151] C.C. Su, M.C. Lu, S.L. Wang, Y.H. Huang, Ruthenium immobilized on Al_2O_3 pellets as a catalyst for hydrogen generation from hydrolysis and methanolysis of sodium borohydride, RSC Adv. 2 (2012) 2073–2079.

[152] E. Keçeli, S. Özkar, Ruthenium(III) acetylacetonate: a homogeneous catalyst in the hydrolysis of sodium borohydride, J. Mol. Cat. A Chem. 286 (2008) 87–91.

[153] J.S. Zhang, W.N. Delgass, T.S. Fisher, J.P. Gore, Kinetics of Ru-catalyzed sodium borohydride hydrolysis, J. Power Sources 164 (2007) 772–781.

[154] X. Xie, Y. Li, Z.Q. Liu, M. Haruta, W. Shen, Low-temperature oxidation of CO catalysed by Co3O4 nanorods, Nature 458 (2009) 746–749.

[155] Y. Karataş Y, A. Aygun A, M. Gülcan M, F. Şen F, A new highly active polymer supported ruthenium nanocatalyst for the hydrolytic dehydrogenation of dimethylamine-borane, J. Taiwan Chem. Eng. 99 (2019) 60–65.

[156] N. Zhan, G. Liu, Y. Sun, Y. Wang, J. Yan, X. Liu, H_2 Evolution upon hydrolysis of ammonia-borane catalyzed by porphyrin stabilized nanocatalysts, Catal. Lett. 151 (2021) 2272–2278.

[157] G. Guella, C. Zanchetta, B. Patton, A. Miotello, New insights on the mechanism of palladium-catalyzed hydrolysis of sodium borohydride from 11B NMR measurements, J. Phys. Chem. B 110 (2006) 17024–17033.

[158] R. Peña-Alonso, A. Sicurelli, E. Callone, G. Carturan, R.A. Raj, Picoscale catalyst for hydrogen generation from $NaBH_4$ for fuel cells, J. Power Sources 165 (2007) 315–323.

[159] S. Ozkar, M. Zahmakıran, Hydrogen generation from hydrolysis of sodium borohydride using Ru(0) nanoclusters as catalyst, J. Alloy. Compd. 728 (2005) 404–406.

[160] F. Fu, C. Wang, Q. Wang, A.M. Martinez-Villacorta, A. Escobar, H. Chong, X. Wang, S. Moya, L. Salmon, E. Fouquet, J. Ruiz, D. Astruc, Highly selective and sharp volcano-type synergistic Ni_2Pt@ZIF-8-catalyzed hydrogen evolution from ammonia borane hydrolysis, Chem. Sci. 8 (2017) 781–788.

[161] R. Retnamma, A.Q. Novais, C.M. Rangel, Kinetics of hydrolysis of sodium borohydride for hydrogen production in fuel cell applications: a review, Int. J. Hydrog. Energy 36 (2011) 9772–9790.

[162] G. Guella, B. Pattton, A. Miotella, 11B Kinetic features of the platinum catalyzed hydrolysis of sodium borohydride from NMR measurements, J. Phys. Chem. C 111 (2007) 18744–18750.

[163] S.B. Kalidindi, U. Sanyal, B.R. Jagirdar, Nanostructured Cu and Cu@Cu_2O core shell catalysts for hydrogen generation from ammonia–borane, Phys. Chem. Chem. Phys. 10 (2008) 5870–5874.

[164] H. Ma, C. Na, Isokinetic temperature and size-controlled activation of ruthenium-catalyzed ammonia borane hydrolysis, ACS Catal. 5 (2015) 1726–1735.

[165] N. Kang, Q. Wang, R. Djeda, W. Wang, F. Fu, M.M. Moro, M.D.L.A. Ramirez, S. Moya, E. Coy, L. Salmon, J.L. Pozzo, D. Astruc, Visible-light acceleration of H_2 evolution from aqueous solutions of inorganic hydrides catalyzed by gold-transition-metal nanoalloys, ACS Appl. Mater. Interfaces 12 (2020) 53816–53826.

[166] W. Chen, J. Shen, Y. Huang, X. Liu, D. Astruc, Catalyzed hydrolysis of tetrahydroxydiboron by graphene quantum dot-stabilized transition-metal nanoparticles for hydrogen evolution, ACS Sustain. Chem. Eng. 8 (2020) 7513–7522.

[167] H. Zhang, L. Zhang, L.A. Rodríguez-Pérez, W. Miao, K. Chen, W. Wang, Y. Li, S. Hana, Carbon nanospheres supported bimetallic Pt-Co as an efficient catalyst for $NaBH_4$ hydrolysis, Appl. Surf. Sci. 540 (2021), 148296.

[168] A. Dutta, C. Nidhi, A. Amitabha, A. De, Hydrolysis of sodium borohydride using Ru–Co-PEDOT nanocomposites as catalyst, Chem. Eng. J. 264 (2015) 531–537.

[169] C.W. Yoon, P.J. Carroll, L.G. Sneddon, J. Am. Chem. Soc. 131 (2009) 855–864.

[170] M. Rakap, S. Özkar, Hydrogen generation from the hydrolysis of ammonia-borane using intrazeolite cobalt(0) nanoclusters catalyst, Int. J. Hydrog. Energy 35 (2010) 3341–3346.

[171] M. Rakap, The highest catalytic activity in the hydrolysis of ammonia borane by poly(N-vinyl-2-pyrrolidone)-protected palladium–rhodium nanoparticles for hydrogen generation, Appl. Catal. B 163 (2015) 129–134.

[172] A. Abhay, V. Kotkondawar, S. Rayalu, Enhanced H_2 production from dehydrogenation of sodium borohydride over the ternary $Co_{0.97}Pt_{0.03}$/CeOx nanocomposite grown on CGO catalytic support, RSC Adv. 10 (2020) 38184–38195.

[173] B. Liu, A. Rose, N. Zhang, Y.Y. Hu, M. Ma, Efficient Co-nanocrystal-based catalyst for hydrogen generation from borohydride, J. Phys. Chem. 121 (2017) 12610–12616.